Petrology, geochemistry and thermobarometry of the northern area of the Flamenco pluton, Coastal Range batholith, northern Chile. A thermal approach to the emplacement processes in the Jurassic andean batholiths.

Natalia Rodríguez[a], Juan Díaz-Alvarado[a,]*, Carmen Rodríguez[b], Karl Riveros[a], Paulina Fuentes[a]

[a] *Departamento de Geología, Universidad de Atacama, Copayapu 485, Copiapó, Chile*

[b] *Unidad Asociada de Petrología Experimental, CSIC-Universidad de Huelva, Campus El Carmen, 21071 Huelva, Spain*

ABSTRACT

The Flamenco pluton is part of a N-S alignment of Late Triassic to Early Jurassic intrusive belt comprising the westernmost part of the Coastal Range batholith in northern Chile. The Jurassic-Cretaceous voluminous magmatism related to subduction in the western active continental margin of Gondwana is emplaced in the predominantly metasedimentary Paleozoic host-rocks of the Las Tórtolas formation, which in the northern area of the Flamenco pluton present an intense deformation, including the Chañaral mélange.

Geochemically, the Flamenco pluton shows a wide compositional variability (SiO_2 between 48wt % and 67wt %). Gabbros, Qtz-diorites and tonalites, mesocratic and leucocratic granodiorites are classified as calc-alkaline, calcic, magnesian and metaluminous magmatism. Flamenco granitoids define cotectic linear evolution trends, typical of magmatic fractionation processes. Geochemical trends are consistent with magmas evolved from undersaturated and low-pressure melts, even though the absence of transitional contacts between intrusive units precludes in-situ fractionation. Although some granodioritic samples show crossed geochemical trends that point to the compositional field of metasediments, and large euhedral prismatic pinnite-biotite crystals, typical Crd pseudomorph, are observed in contact magmatic facies, geochemical assimilation processes are short range, and the occurrence of host-rocks xenoliths is limited to a few meters from the pluton contact.

A thermal approach to the emplacement process has been constrained through the thermobarometric results and a 2D thermo-numerical model of the contact aureole. Some Qtz-diorites and granodiorites located in the north area of the pluton exhibit granulitic textures as Hbl-Pl-Qtz triple junctions, poikiloblastic Kfs and Qtz recrystallization. The Hbl-Pl pairs have been used for the thermobarometric study of this metamorphic process, resulting granoblastic equilibrium

temperatures between 770 and 790 °C, whereas Hbl-Pl pairs in domains that preserve the original igneous textures yield temperatures above 820 °C . This is characteristic of self-granulitization processes during the sequential emplacement of composite batholiths.

In addition, the thermal modelling was used in order to compare the expected and observed thermal contact aureole of the intrusive body. Model P-T conditions have been established between 3 and 4 kbars (extracted from the thermobarometric results), and temperatures between 1159 °C (*liquidus* temperature for a tonalitic composition) and 992 ºC (fixed at the rheological threshold of a 50% crystal fraction). The thermal modeling estimates a homogeneous contact aureole, where the established temperatures for the melting reactions in the host-rocks are located at distances between 200 and 650 m from the magma chamber boundary, whereas the temperatures for Crd stabilization extend 1500 m far from the contact in the case of the emplacement at *liquidus* temperatures and 4 kbars. According to field observations, the contact aureole presents a scarce development in the northern area of the Flamenco pluton, with few migmatite outcrops and less than 1 Km in thickness for Crd-schists. However, in the southern contact, partially melted rocks are described at distances up to 2 km from the Flamenco pluton boundary.

The processes of self-granulitization and the differences between the observed and calculated (by the thermal modeling of one single pulse) contact aureole suggests a process of incremental emplacement for the Flamenco pluton, by accretion of magmatic pulses from north to south (in its current position), where the thermal maturity reached through the repeated magmatic intrusion generates a more extensive area of high-grade metamorphism.

Keywords: thermal modelling, contact aureole, self-granulitization, Coast Range batholith, northern Chile

1.- Introduction

The Flamenco pluton is part of the numerous and discontinuous outcrops of Late Paleozoic to Mesozoic igneous rocks emplaced in the Paleozoic metasedimentary basement which, taken together, form the so-called Coastal Range in northern Chile (Brook et al., 1986). Specifically, granitoids that make up the Flamenco intrusive body are framed in the voluminous calc-alkaline arc magmatism of Jurassic-Cretaceous age owing to the Coastal Range batholith. This magmatism was generated along the western Gondwana margin because of the reactivation of subduction in an

extensional to transtensional tectonic regime in the Early Jurassic (Mpodozis and Kay, 1990; Dallmeyer et al., 1996; Grocott and Taylor, 2002).

The subduction in convergent margins has been proposed as the most efficient and sustainable mechanism to generate new continental crust since the Late Proterozoic (Kemp and Hawkesworth, 2003; Castro, 2014), supported by the statistical frequency of U-Pb zircon ages obtained from the continental crust (Condie, 1998, 2000). Cortical growth is directly related to the magmatism associated with subduction zones that are active without pronounced breaks, such as on the western margin of South America during the Andean cycle (Von Huene and Scholl, 1991 Plank and Langmuir, 1998). Therefore, subduction is the main engine for calc-alkaline magmatism and the formation of large cordilleran-type batholiths (Wyllie et al., 1976; Wyllie, 1977). Low water content, hybrid geochemical signatures and high compositional homogeneity are essential features for assessing the conditions and the sources of cordilleran magmatism (Castro, 2013; Burgisser and Bergantz, 2011). Several models have been proposed to generate these geochemical characteristics, such as the repeated intrusion of basaltic sills in a fertile lower crust (Annen y Sparks, 2002), the partial melting of crustal andesitic protoliths controlled by peritectic paragenesis ("PAE": peritectic assemblage entraintment) (Clemens et al. 2011, 2012), and the off-crust generation from partial melting of metasediment-MORB mélanges or cold diapirs that are finally relaminated to the continental crust and separated into residues (lower crust mafic granulites) and liquids (cordilleran magmatism) (Castro 2013, 2014).

Re-thinking the emplacement and formation of large batholiths through geochronological data and detailed field and seismic studies (Glazner et al., 2004; Coleman et al., 2004) has outpaced old ideas about instantaneous balloon-like plutons (Bohrson and Spera, 2001; Huppert and Sparks, 1998). Although the batholith building is nowadays a controversial subject among the petrology community, many authors propose that incremental growth of composite batholiths is accomplished through small discrete magmatic pulses or batches (i. e., Annen, 2011; Michaut and Jaupart, 2011; Menand et al., 2015) over more than 10^5 years according to new and precise geochronological studies (i. e., Miller et al., 2007, 2011; Díaz-Alvarado et al., 2013), as has been confirmed by incorporating the influence of temperature on the crystallinity and thermal conductivity, and the depths of emplacement to the models (Gelman et al., 2013). The positive correlation between the period of amalgamation and the size of the batholith has highlighted that the availability of magmas in the crust depends on the fertility of both mantle and crust and the convergence dynamics between plates in convergent margins (Saint Blanquat et al, 2011). Thus, according to thermo-numerical models, magmatic addition rates in extensional arcs are higher than in continental margins with stable or compressive geodynamic regimes (Vogt et al., 2012). However, calculations for estimating

103 the volumes of magma fluxes ascending to the upper crust are particularly difficult to determine.
104 Although subduction is active during tens of millions of years, volumetrically, most of the magma
105 is emplaced during periods of 10 to 30 Ma (Paterson et al., 2011).
106 Processes such as magma differentiation, fractionation, high-grade metamorphism and assimilation
107 of host rocks may occur at the emplacement level, not only in the source area, and they are closely
108 related to the style and emplacement rate of the magma chamber (Annen, 2011). Hence, variations
109 in magma fluxes and the incubation period required to establish high-grade conditions account for
110 the simultaneous presence in magmatic arcs of both magma-magma relations during the main
111 intrusive phases and self-granulitization processes in earlier magmatic pulses (Annen and Sparks,
112 2002; Castro et al, 2014). The shape and thickness of the thermal aureole associated with a growing
113 igneous body during the amalgamation of magma pulses depends on the emplacement constraints
114 described above in addition to the thermal and mineralogical characteristics of the host rocks
115 (Annen, 2011). Although the volume and the spatial distribution of magmatic increments rather
116 than the shape of individual pulses determines the sequential growth of large batholiths (Paterson et
117 al., 2011), most models propose small tabular bodies with horizontal disposition (i. e., Annen et al.,
118 2006, 2011; Díaz-Alvarado et al., 2013). Accordingly, the development of the metamorphic aureole
119 depends on the relative location of successive laminar pulses, and an irregular and non-concentric
120 aureole would be formed during over-, under- or intra-accretion (Annen, 2011; Menand et al.,
121 2010). Therefore, the formation of high-grade metamorphic areas in the host-rocks during the
122 batholithic sequential emplacement depends on the temperatures and periodicity of intrusive magma
123 fluxes and the location of crustal rocks in relation to the intrusive sheets; these are mostly related to
124 crustal-scale tectonic structures that can increase and sustain high-grade and hyper-solidus
125 conditions in the host rocks and residual liquids, respectively (Díaz-Alvarado et al., 2012, 2013;
126 Annen, 2011).
127 The degree of development of the metamorphic aureole and tectonics influence the anisotropy and
128 the disgregation of the host rock, a major control in the magnitude of the interaction processes
129 between the intrusive magma and crustal rocks at the emplacement level. Mechanical mixing and
130 reactive bulk assimilation account for considerable in-situ geochemical variations (i. e., Beard et al.,
131 2005; Saito et al., 2007; Díaz Alvarado et al., 2011).
132 In this study, we present the first complete geochemical data from Flamenco pluton granitoids.
133 Field relations, petrographic features, geochemistry, thermobarometric data and thermal modeling
134 allow us to determine the geochemical relations between the intrusive units and the extent of the
135 interaction processes that occurred between intrusive magmas and metasedimentary host-rocks. In

addition, we obtain a thermal setting to assess the batholith building processes during the emplacement of the Jurassic-Cretaceous magmas in northern Chile.

2.- Geological setting

The geology of the Coastal Range batholith in northern Chile has been controlled by eastward subduction along the western margin of South American plate and global tectono-magmatic events since the Late Paleozoic. Following an almost total cessation of subduction during the Triassic-Early Jurassic rifting stage, the subsequent fragmentation of Gondwana caused a period of subduction reactivation and the earliest evidence of the magmatic arc development (~183 Ma), established in a crustal extensional context (Ramos, 1999; Charrier et a., 2007; Mpodozis and Ramos, 2008). During the NW-SE trending oblique convergence of the Phoenix and the South American plates, the high angle of subduction favored the negative velocity of trench roll-back (Mpodozis and Ramos, 2008). Thus, a magmatic arc was formed, located in the current coastal range (Fig. 1a, b).

Magmatic activity during the Triassic Pre-Andean cycle fits into a stationary period during the final consolidation of Pangea (Vilas and Valencio, 1978). This created a new tectonic context along the western margin of Gondwana that favored heat accumulation in the upper mantle and melting conditions in the lower crust, generating NNW-SSE trending elongated basins and large volumes of magma along the coast of northern Chile (Berg and Breitkreuz, 1983; Berg et al. 1983). In the study area, Late Permian magmatism is represented by granitic plutons called Quebrada del Castillo and Quebrada Quiscuda (264-244 Ma: Rb-Sr, Berg and Baumann, 1985; K-Ar, Ulriksen, 1979; K-Ar, Naranjo and Puig, 1984). Triassic intrusive magmas are leucocratic S-type granitoids, with $^{87}Sr/^{86}Sr$ between 0.7103 and 0.7172 (Berg y Baumann, 1985), and correspond to the plutons Pan de Azúcar (230 Ma: U-Pb, Berg and Baumann, 1985), Cerros del Vetado (217 Ma: U-Pb, Berg and Baumann, 1985) and Capitana (199-215 Ma: K-Ar and U-Pb, Godoy and Lara, 1998).

Subduction reactivation led to the formation of a Jurassic-Cretaceous magmatic arc, parallel to the west margin of Gondwana that has gradually migrated eastward and is located in the Principal Cordillera. This arc primarily forms the Coastal Cordillera batholith and is mostly composed of a calc-alkaline plutonic complex formed by hornblende-biotite gabbros, diorites, tonalites to granodiorites, and proportionally less granites (Dallmeyer et al. 1996) in addition to andesitic, basaltic and dacitic volcanic rocks (González and Scheuber, 1997). Plutonic complexes were emplaced in Late Paleozoic metasedimentary basement rocks and Permian-Triassic plutonic

complexes. Between 25º30'S to 26º30'S (Fig. 1a, b), Jurassic plutons show a high compositional variability and correspond to the Bufadero and the Peralillo plutons (no data available), the Cerro Castillo (201,6 Ma: Rb-Sr, Berg y Baumann, 1985), the Barquito (193-204 Ma: K-Ar, Farrar et al., 1970; K-Ar, Díaz, 1986; Rb-Sr, Berg y Breitkreutz, 1983), the Las Ánimas (164-148 Ma: Rb-Sr, Berg y Breitkreutz, 1983; U-Pb, Berg y Breitkreutz, 1983; $^{40}Ar/^{39}Ar$, Dallmeyer et al., 1996; K-Ar, Díaz, 1986) and the Flamenco (described below) plutons. Volcanic rocks derived from the arc activity are found in the La Negra formation and the Punta del Cobre Group. These are basaltic to andesitic lavas interbedded with marine sedimentary rocks (Godoy and Lara, 1998). An extensional tectonic regime was maintained until the Late Cretaceous (Mpodozis y Ramos, 2008; Charrier et al., 2007).

The metasedimentary basement in the study area corresponds to the Las Tortolas formation, which has been defined as a turbiditic sedimentary succession developed at the shelf margin and talus environments (Bell, 1982). This formation comprises low to medium metamorphic grade mudstones and sandstones (mainly phyllites and quartzites) with minor limestones, conglomerates, volcanic rocks ("pillow" lavas) and pelagic cherts (Bell, 1982; 1987; Ulriksen, 1979; Naranjo and Puig, 1984; Godoy and Lara, 1998). The Las Tórtolas formation is included in the Chañaral Epi-metamorphic Complex (CECh) (Godoy and Lara, 1998), forming two elongated NNE to SSW strips separated by a 100 km wide graben filled with younger sediments (Levi and Aguirre, 1981). Several depositional ages have been proposed for the turbidite rocks based on their fossil content, from Ordovician to Devonian (Bell, 1982; Naranjo and Puig, 1984), Carboniferous (Bahlburg et al., 1986), and Carboniferous to Permian (Bell, 1987).

The Las Tórtolas formation was tectonically deformed and subjected to greenschist facies metamorphism (Miller 1970; Aguirre et al. 1972) during the Late Carboniferous or Early Permian. However, the formation includes an extremely deformed domain called Chañaral Melange that is defined as blocks of sandstone in a pelitic matrix (Bell, 1982; Bell, 1987). This deformation has been linked to a tectonic context of an accretionary wedge resulting from subduction towards the NE and the overlapping of several complex deformational events affecting unlithified sediments (Bell, 1987).

The Early Jurassic Flamenco pluton (Fig. 1c) intrudes the Las Tórtolas formation and corresponds to a sub-circular body of approximately 15 kilometers in diameter comprising calc-alkaline Hbl-Bt tonalites to granodiorites, with minor Qtz-diorites and gabbros (Grocott et al., 1994), including orbicular gabbros (Godoy, 1997). The Flamenco pluton is intruded by conjugated sets of andesitic NW-SE and NE-SW dykes (Dallmeyer et al., 1996). The estimated ages for the pluton are between 201 and 186 Ma (Berg y Breitkreuz, 1983, Brook et al., 1986, Dallmeyer et al., 1996). The

correlation between age and Hbl-blocking temperatures suggests magma emplacement in shallow cortical levels followed by rapid cooling (Dallmeyer et al., 1996).

3.- Field relations and sample descriptions.

The Flamenco pluton is emplaced in pelitic and quartzitic metasedimentary rocks of a highly deformed domain of the Las Tórtolas formation, which includes minor interbedded limestones and conglomerates (Fig. 1c). A meta-volcanosedimentary sequence outcrops at the northern contact of the Flamenco pluton (Fig. 1d). It is mainly comprised of basaltic and dacitic lavas with interbedded quartzites and rare phyllites, and culminated at top with andesitic blocks and glass shards in a rhyolite mass. These rocks have not been previously described but are out of the scope of this study. The north contact of the intrusive body has an irregular morphology with a W-E orientation and an approximately 18 km extension (Fig. 1d). According to satellite images and studies in other areas of the intrusive complex (i. e., Grocott and Taylor, 2002) (Fig. 1c), most of the contacts are sharp and steeply dipping. On a large scale, there are scarce kilometric fragments of host metasediment that are wholly or partially isolated within the intrusive granitoids (Fig. 1c). On a smaller scale, numerous metasedimentary irregularly shaped xenoliths of different sizes are hosted in the granitoids (Fig. 2a), always in the first few meters from the contact. Inland, only microgranular Qtz-dioritic enclaves are observed.

The Las Tórtolas formation shows three distinct domains in the study area according to their structural characteristics. The western area belongs to the melange facies (Fig. 1d), where the ellipsoidal quartzite objects included in a phyllite matrix show a primary NW-SE stretching lineation with low dips (between 5 and 20º). Foliations, where they can be measured, are NW-SE trending but SW and NE dipping. This is consistent with previous studies performed in the melange facies in other areas not directly influenced by the intrusive magmas (Bell, 1987). Melange textures are not present in the eastern area, but it features a strong deformation. Major structures are straight or slightly inclined SW vergent folds with N165E trending axial traces. Quartzites and some volcanic layers show boudinage and pinch and swell structures, which are further subjected to a second deformation phase causing auto-thrusting of the previously stretched or separate layers (Fig. 2b). In the eastern area, the structure is dominated by large lateral extension thrusts and associated propagation folds. These folds are verging to the SW and have identical axial traces defined by straight folds (Fig. 1d). Late transcurrent faults with N60E and N140E preferred orientations cut units and structures described above.

238 The contact aureole shows an irregular development in the metasedimentary formation in the north
239 contact of the Flamenco pluton. Its thickness ranges from 50 to 800 m, dominated by Crd-schist
240 (mineral abbreviations after Kretz, 1983) and to a lesser extent, migmatitic hornfelses with scarce
241 leucosome bands or partial melting percentage (Fig. 2c). Migmatites are mainly developed in the
242 pelitic lithologies, and from the contact into the metasedimentary formation, the metamorphic
243 sequence is comprised by migmatitic hornfelses, Crd-schists and Crd-phyllites. In other areas of the
244 contact aureole, this sequence is inverted (eastern part of the study area, Figure 1d) where low-
245 grade rocks (Crd-absent phyllites) are near the intrusive body, and the metamorphic grade increases
246 toward the host rock. Changes in the metamorphic grade also appear to be tectonically controlled by
247 NW-SE trending structures within the metasedimentary formation, resulting in strips of Crd-schist
248 that progressively vary to low grade phyllites. Where Crd-schist attain a medium to large grain size,
249 cordierites show a preferred orientation evidenced by a N150E trending plastic stretching lineation
250 (Fig. 2d).
251 The Flamenco pluton shows large petrological variability in the study area, located in its northwest
252 domain (Fig. 1b, c), which is representative of the entire pluton. The areas nearer the contact with
253 the metasedimentary host rocks are dominated by Hbl Qtz-diorite to tonalite granitoids, and
254 mesocratic granodiorites mostly outcrop toward the interior of the intrusive body. Several intrusive
255 sheets of gabbros and leucocratic granodiorites are disposed in an approximate NNW-SSE
256 orientation, presenting sharp contacts, self-enclaves and dykes in the host tonalites. Included in
257 gabbroic facies, the presence of a small lensoidal shaped body of orbicular gabbros (Fig. 1d, 2e) is
258 noteworthy. Several apophyses associated with the Flamenco pluton are isolated in the
259 metasedimentary host rocks. The presence of an elongate dyke-like body of granodioritic
260 composition that shows large idiomorphic prismatic crystals of biotite-pinnite (Fig. 2f) is notable.
261 The main mineralogical and textural characteristics of the identified magmatic facies are listed
262 below.
263
264 *3.1 Petrographic descriptions*
265
266 *Gabbros (NM-4)*
267 This unit is a fine- to medium-grained mesocratic rock that displays an isotropic fabric and
268 phaneritic/hypidiomorphic textures. Its mineralogical composition is dominated by euhedral to
269 subhedral, twinned and zoned Pl crystals (~65 vol. %) with a grain size of 0.75-2.5 mm that are
270 weakly altered to sericite, calcite and epidote. Frequently, secondary Mg-rich Chl (~1 vol. %) fills
271 the microfractures and the intersticial spaces developed in the Pl crystals. These rocks also contain

subhedral to anehdral Hbl crystals (~35 vol. %) with a grain size of 0.6-5 mm that are moderately altered to Mg-rich Chl, whereas scarce secondary Bt (< 1 vol. %) along the Hbl cleavage is also observed. Opx is present in the inner areas of Hbl aggregates (Fig. 3a). Opaque minerals and Qtz represent less than 2 vol. % of these rocks. A poikilitic texture is observed in the Hbl where it is enclosed by small Pl crystals.

Qtz-diorites (NM-3)

This unit is a medium-grained mesocratic rock showing an isotropic fabric and phaneritic/hypidiomorphic textures. Mineralogical composition of this rock unit is strongly dominated by euhedral to subhedral Pl (~60 vol. %) ranging from 0.25 to 3 mm, Hbl (~20 vol. %) with a grain size of 0.5-3.5 mm, Qtz (~7 vol. %) and Bt (~5 vol. %) showing grain sizes of 0.75-2 mm (Fig. 3b). Pl crystals are weakly altered to sericite and calcite, whereas Bt is strongly altered to Fe-rich Chl and moderately replaced by Ep. Subhedral Sph, Ap and opaque minerals represent the main accessory phases in these rocks. In concrete domains, corroded Opx grain boundaries and triple junctions between Hbl, Pl and Qtz are observed.

Tonalites (NM-1 and NM-8)

Tonalites consists of a fine- to medium-grained leucocratic rocks with an isotropic fabric and faneritic/equigranular texture (Fig. 3c). These rocks exhibit a wide range of alteration degree. Primary minerals in fresh tonalite include subhedral Pl (~55 vol. %) with a grain size of 0.5-1.5 mm, subheudral to anhedral Bt (~10 vol %) with a grain size of 0.3-1.6 mm, subheudral to anhedral Hbl (2 vol. %) with a grain size of 0.5-2.75 mm, and anhedral Qtz (~25 vol %). Accessory minerals are represented by sphene and opaque minerals.

Leucocratic granodiorites (NM-5 and NM-7)

Rocks from this unit exhibit a fine-grained hypidiomorphic, equigranular and phaneritic textures in which the mineralogical composition is dominated by subhedral Pl crystals (~50 vol. %), that are between 0.5 and 1.75 mm, anhedral Qtz (~25 vol. %) with crystals smaller than 1.5 mm, subhedral Kfs (~10 vol. %) ranging from 0.25 to 1.5 mm and anhedral to subhedral Bt (~7 vol. %) with a grain size of 0.5-1.7 mm (Fig. 3d). The main accessory phases in these rocks are represented by euhedral to subheudral Sph that have crystals smaller than 1 mm and anhedral opaque minerals smaller than 0.25 mm.

Mesocratic granodiorites (NM-6)

Mesocratic granodiorites show two main textural domains. Where igneous textures are present, they present an isotropic fabric and equigranular, hypidiomorphic and fine-grained phaneritic textures. However, granoblastic textures are dominant over wide areas, where Hbl-Pl-Qtz triple junctions (Fig. 3e), poikiloblastic Kfs (Fig. 3f) and an extensive recrystallization are observed (Fig. 3e, f). The mineralogical composition is dominated by subhedral and twinned Pl (~45 vol. %) with crystals smaller than 1.5 mm, anhedral Qtz (~35 vol. %) with a grain size of 0.15-0.5 mm, subhedral Bt (~10 vol. %) ranging from 0.25 to 1.25 mm, subheudral Hbl (~5 vol. %) with a grain size of 0.25-2.5 mm and subheudral Kfs (~2-3 vol. %) showing a grain size of 0.25-1.5 mm. Scarce and small opaque crystals represent the main accessory phases in these rocks.

Crd-granodiorites (NM-2A)

This unit exhibits a distinctive glomeroporphyritic texture with medium-grained phenocrysts and xenocrysts (smaller than 7 mm) that represent approximately 55 vol. % of these rocks (Fig. 3g). These medium size crystals comprise subheudral to anhedral zoned and twinned Pl (~35 vol. %), polycrystalline rounded Qtz xenocrysts (~10 vol. %) (Fig. 3g), Kfs (~5 vol. %), Hbl (~3 vol. %) and Bt (~2 vol. %). Phenocrysts of Hbl are moderately to strongly affected by secondary and fine-grained biotite. Clots of fine-grained Bt, Kfs and quartz occur within prismatic and subhedral Bt phenocrysts, which mostly show hexagonal sections. The groundmass (~45 vol. %) shows crystals smaller than 0.25 mm and is completely obliterated by a secondary fine-grained assemblage of Qtz-Pl (~30 vol. %) and Bt (~10 vol. %), whereas Kfs crystals (~5 vol. %) also occur. The main accessory phases are related to zircon and opaque minerals.

Crd-schists (NM-2B)

Crd-schists are the most representive facies in the metasedimentary host-rocks. They are characterized by a grano-lepidoblastic texture related to a millimetric alternance of quartz-rich (leucocratic) and mica-rich (mesocratic) continuous to discontinuous bands. The limits of these mineralogical bands are sinuous, sharp and well-defined (Fig. 3h). Leucocratic bands mainly comprise anhedral Qtz crystals (~90-95 vol. %) ranging from 0.025 to 0.5 mm and minor amounts of fine anhedral to subhedral Ms and Bt (~5-10 vol. %), with a grain size smaller than 0.25 mm. The mesocratic bands are dominated by a mix of subhedral fine-grained Bt (~60 vol. %), anhedral Qtz (~10 vol. %) and anhedral Crd (~30 vol. %), in which most of the crystals are smaller than 0.05 mm. Bt crystals display an incipient orientation. Opaque minerals (~2-3 vol. %) show an average grain size of 0.025 mm and occur only in the mesosome bands.

4.- Geochemistry

4.1 Sampling and analytical techniques

Selected samples for the geochemical study of the Flamenco pluton were collected along the northern contact of the intrusive body with metasedimentary rocks of the Las Tórtolas formation (Fig. 1d). Eight samples were chosen for major and trace element analyses to characterize the main facies composing the pluton in the study area. Geochemical data have been plotted to determine their geochemical and genetic relationships and to point some clues about the magmatic processes involved during the generation, ascent and emplacement of the magmas. Additionally, the selection of sampling points, with different spatial and textural relationship with the host rocks (presence of enclaves or exotic mineralogies) allows us to assess the extent of the processes of interaction between the intrusive magmas and the metasedimentary rocks at the emplacement level. The geochemical data of the studied samples are presented in figures 4 to 8 and in table 1. For comparative data, two plutonic complexes of the Coastal Range Batholith were used. The Lower Cretaceous Copiapó Plutonic Complex (Marschik et al., 2003) and the Lower Jurassic to Lower Cretaceous Limari-Papudo-Illapel batholith (Parada et al., 1999) were selected because of their spatial and geochronological relationship with the Flamenco pluton, and the scarcity of geochemical data along the Coastal Range batholith. Additionally, two referenced examples of cordilleran batholiths are projected in variation diagrams (Patagonia batholith: Hervé et al., 2007; Pankhurst et al., 1999; and Peninsular Range batholith: Lee et al., 2007).

Approximately 3 kg of fresh rock was collected from each outcrop. Samples were crushed and milled to a fine powder in steel cups. Major elements were analyzed by X-ray fluorescence (XRF), with a Siemens SRS-3000 at the Universidad Católica del Norte (Chile). The precision of the XRF technique is between 0.1% and 1%. Trace elements, including rare earth elements (REE), were analyzed by inductively coupled plasma atomic emission spectrometry (ICP-AES) with a Perkin-Elmer Optima 2000 DV model at the Universidad Católica del Norte (Chile). The sample is dissolved in a Claisse M4 Fluxer with a Na_2CO_3 – $Li_2B_4O_7$ mixture. This residue is dissolved in approximately 4 ml of HNO_3 and distilled water, and the solution is passed through a fractionation column containing an ion exchange resin (Dowex 50-WX8) separating the REEs, which are then eluted with 50 ml of HNO_3 6N and 20 ml HNO_3 8N. To achieve accuracy and precision with the method, two international standards (GA and GH) from Centre National de la Recherche Scientifique (CNRS, France) are used.

374

375 *4.2 Geochemistry results*

376

377 The Flamenco granitoids present a high percentage of CaO with respect to alkalis (Fig. 4a),
378 showing an almost linear trend from gabbros to tonalites and granodiorites. Together, the samples
379 describe a magnesian, metaluminous and calcium magmatic series (Fig. 4b, c, d). Both ASI vs. SiO_2
380 and MALI diagrams (Fig. 4c, d) (Frost et al., 2001) show that the most SiO_2 rich samples point to
381 peraluminous and calc-alkalic fields, respectively, denoting alkali and alumina enrichment for the
382 most evolved terms (Fig. 4b, c, d). According to the Nb vs. Y tectonic discrimination diagram (Fig.
383 4e) (Pearce et al., 1984), Flamenco granitoids belong to syn-collisional volcanic arc granitoids.
384 Harker diagrams show mainly linear trends for the magmatic facies that form the north area of the
385 Flamenco pluton, with a wide SiO_2 range (48 to 67%) from gabbros to granodiorites (Fig. 5). TiO_2,
386 Al_2O_3, MgO, FeO y CaO describe negative trends versus silica, whereas K_2O increases and Na_2O
387 shows a flat or slightly positive pattern. Nevertheless, granodiorites display a more scattered
388 distribution for some elements (K_2O, Na_2O and Al_2O_3, Fig. 5). The studied samples match the
389 compositional trends drawn by typical calc-alkaline cordilleran batholiths. Only the Copiapó
390 Plutonic Complex shows a different geochemical pattern, indicating the higher alumina and alkalis,
391 and lower CaO and MgO contents for the same SiO_2 ranges.
392 Figure 6 shows a pseudoternary system defined by Opx-An-Or (Díaz-Alvarado et al., 2011; Castro,
393 2013). This projection is particularly significant for visualizing magmatic processes in natural rocks
394 and experimental data, according to which different fields have been defined by T, P and H_2O
395 conditions for the generation and the evolution of granitic melts (Castro, 2013 and references
396 therein). Flamenco pluton granitoids trace a cotectic-like evolution from gabbros and Qtz-diorites to
397 tonalites and granodiorites. This trend matches the field described for undersaturated and low-
398 pressure melts, and, as shown in the previous diagrams, are consistent with comparative cordilleran
399 granitoids. Fractionation or cotectic trends are crossed by transverse lines defined by some
400 granitoids from the Flamenco pluton and comparative samples. These are evident in samples from
401 the Copiapó Plutonic Complex and the Limarí-Papudo-Illapel batholith, and in slight deflection, in
402 some granodiorites from the Flamenco samples. Granodiorites (NM-2 and NM-6) outline transverse
403 trends pointing to the compositional fields of graywackes and pelites, in which the metasedimentary
404 rocks of the Las Tórtolas formation (Fig. 6 and 7a) are represented. Anyway, Flamenco samples
405 from Qtz-diorites to granodiorites show a general linear trend and close geochemical characteristics
406 with calc-alkaline cordilleran magmatism (Fig. 7b and c).

Rb and other trace elements associated with K_2O are enriched in more differentiated samples without entailing a variation of the alumina saturation index (ASI) (Table 1, Fig. 7d), which remains constant in all samples, with slight variations in some granodiorites (NM-2, Crd-Granodiorites). The variance between LREE and HREE is represented by the relationship between Lu* and the La*/Lu* ratio (Fig. 7e). The La values are almost identical for all the studied samples. However, the Lu values are lower and, therefore, the LREE/HREE are greater for granodiorites compared to less evolved granitoids. Spider diagrams (Fig. 8a, b) are employed using Thompson MORB normalization and are consistent with average values given by Kelemen et al. (2003) for typical continental arc andesites. The Flamenco pluton samples show typical depletion of Nb and Ti, more outstanding in granodiorites (Fig. 8b), and enrichment in Ba, Rb and K that characterize arc setting magmatism.

5.- Thermobarometry and thermal modeling

5.1 Thermobarometry

With the aim of estimating temperatures and pressures reached at the emplacement level of the Flamenco pluton and to assess P-T conditions during granoblastic recrystallization described in some intrusive granitoid facies (see Chapter 3), mineral compositions obtained by electron microprobe analyses were used. Two Qtz-dioritic samples (NM-3 and NA-2) were selected for the thermobarometric study (Fig. 9a). According to mineral assemblages found in granitoids comprising the Flamenco pluton, temperatures have been obtained using Hbl–Pl equilibrium after multiple iterations as a function of the pressure. These temperatures are interpreted as cooling temperatures and can be established as a minimum magma temperature during the emplacement process. Furthermore, when the petrographic study indicated that some granodioritic facies have metamorphic textures (NM-6), Hbl-Pl thermobarometry was used to approach the conditions for the granulitization process. All thermometry results are referred to HB2 temperatures calibrated according to the reaction of edenite+albite=richterite+anorthite (Holland and Blundy, 1994). As a first approach, 2 and 4 Kbars have been selected. The presence of Crd and absence of Grt in the metasedimentary pelitic host rocks settle an upper limit of 4-6 Kbars for pressure conditions (Le Breton and Thompson, 1988; Vielzeuf and Holloway, 1988). Calibrations of the Al-in-hornblende barometer (Schmidt, 1992) have also been used, yielding consistent results with randomly selected pressures. Electron microprobe analyses were conducted with a JEOL JXA-8200 SuperProbe at the

441 University of Huelva. A combination of silicates and oxides were used for calibration. The results
442 are shown in Table 2. The compositions of the analyzed Hbl-Pl pairs are shown in Appendix 1.
443 Figure 9 shows BSE images of selected samples for the thermobarometric study. Hbl-Pl pairs in the
444 Qtz-diorite samples (Fig. 9b, c) yield constant temperatures from 820 to 850 ºC for random and
445 calculated pressures, resulting in Schmidt pressures of 3 ±0.15 kbars (Table 2). These results are
446 obtained in equilibrium igneous textures. However, the NM-3 sample shows areas where engulfed
447 Opx, interstitial Hbl and triple junctions between Pl and Hbl (Fig. 9d) are observed. Hbl-Pl
448 temperatures are slightly lower in these areas, between 800 and 820ºC.
449 Leucocratic granodiorites sampled near the Flamenco pluton contact (Fig. 9a) show an almost
450 complete demise of igneous textures because of granoblastic recrystallization observed in these
451 intrusive facies. Qtz-Pl-Hbl triple junctions and interstitial and poikiloblastic Kfs crystallization are
452 dominant over the igneous textures (Fig. 9e, f). Temperatures reached during granulitization are
453 obtained from the Hbl–Pl pairs showing granoblastic textures as a criterion of chemical equilibrium.
454 In areas where the original straight igneous contacts are preserved (Fig. 9e), temperatures
455 approximately 830 °C are maintained. However, where recrystallization processes are evident,
456 temperatures yielded by granoblastic Hbl-Pl pairs are considerably lower (Fig. 9e, f), between 770
457 and 790 °C (Table 2). Calculated Schmidt pressures are higher than those obtained for NM-3 Qtz-
458 diorites, ca. 4 ±0.5 kbars Kbars.
459 The granodioritic intrusive facies with igneous textures show oscillatory zoned Pl.
460 Thermobarometric data calculated between Pl Ca-rich cores (75% An) and zonation absent Hbl,
461 assuming that these phases were previously in equilibrium, give temperatures approximately 900 ºC
462 (Table 2). These results should be considered a minimum of the magma temperatures during the
463 emplacement process, whereas temperatures obtained using Pl external rims (50% An) are lower
464 cooling temperatures.
465

466 *5.2 Thermal modeling*
467

468 *Rationale and model setup*
469 Numerical modeling has been applied to study a wide range of geological processes, as the relation
470 of the magma with the host rock, the residence times of silicic magma chambers, the cooling,
471 emplacement, crystallization and compositional variations of different magma chambers (Annen,
472 2009; Bachmann and Bergantz, 2004; Bea, 2010; Dufek and Bergantz, 2005; Gelman et al., 2014;
473 Gelman et al., 2013; Gutiérrez and Parada, 2010; Koyaguchi and Kaneko, 2000; Molina et al.,

2015). Here, the thermal modeling of cooling magma chambers is used to know the thermal effect on the host rock at different conditions of emplacement.

We have simulated 4 case studies of crystallizing magma chambers at different depths, corresponding to 3 and 4 kbar, diverse temperatures of emplacement (Table 3), and redox conditions of one log unite above the QFM oxygen buffer, by the 2D numerical approach solving conductive cooling by finite difference (Wohletz et al., 1999). The FD mesh consists of elements of 100-meter-size for both magma and host rock. Modeling of phase equilibria is conducted with the Rhyolite-MELTS code (Gualda et al., 2012), in order to know *liquidus* and crystal fraction evolution regarding the different conditions of emplacement. The composition used for thermal modeling is the tonalite NM-8 because of their abundance along the batholith and the proximity to the parental magma according to field observations.

The purpose of this thermal modeling is to establish the extent and shape of the thermal metamorphic aureole caused by magma intrusion. With this aim, we consider two extreme scenarios for the magma emplacement. In one case, the magma is emplaced with a crystal fraction of 0.5 (case studies 1 and 2: Fig. 10a, b). We use this crystal fraction as upper limit above which the rheological properties would inhibit the magma emplacement (Bachmann and Bergantz, 2004). At the opposite end, the magma intrudes as totally liquid, and temperature of emplacement will be the corresponding to the *liquidus* (case studies 3 and 4: Fig. 10c, d). The thermal modeling covers the entire temperature range from the instantaneous emplacement to the solidification of the whole magma. Temperature of emplacement, magma density and specific heat capacity have been set by Rhyolite-MELTS code according the two scenarios proposed here (Table 3). We range the pressure of emplacement from 4 to 3 kbar, according to the thermobarometry data described in the previous section.

The selected geometry for all case studies is tabular with 20 km of width and 2 km of height, corresponding to a constant volume of 62.83 km^3 (Table 3). Thermal properties for the different case studies are given in Table 3. The thermal gradient imposed for the crust is 30 ºC/km (de Silva and Gregg, 2014; Gelman et al., 2013; Huber et al., 2009).

Heat transfer is calculated solved to the conservation of energy:

$$\frac{\partial T}{\partial t} = \nabla \cdot K \nabla T - \boldsymbol{u} \cdot \nabla T + Q \qquad (1)$$

where T is magma temperature, t is time, κ is thermal diffusivity, u is the velocity vector, and Q contains heat sources and sinks. The latent heat of crystallization is included in calculations with a constant value of 350 kJ/kg for silicate phases is assumed (Wohletz et al., 1999):

$$\frac{\partial T}{\partial t} = \frac{Q}{(C_p+1)\Delta T_{SL}} \quad (2)$$

where the latent heat is Q, C_p is the heat capacity and ΔT_{SL} is the temperature interval between *liquidus* and *solidus*.

Thermal conductivity of magma is set at 1.3 and 1.5 W/mºC as initial value depending on the temperature of emplacement (Table 3), and it is considered as dependent on the pressure and temperature according to the equation from (Chapman and Furlong, 1992):

$$K(T,z) = K_0 \frac{(1+cz)}{(1+bT)} \quad (3)$$

where K(T,z) represents the thermal conductivity variation regarding the temperature (t) and depth (z), K_0 is conductivity at 0°C, *c* is the crustal depth constant, and *b* is the thermal constant for the upper crust.

Crustal density is fixed at 2800 kg/m^3. Magmatic density and specific heat are estimated by Rhyolite-MELTS code according to the magmatic conditions of emplacement (Table 3). The heat capacity (C_p) for crust is also assumed as constant (1390 J/kgºC; Gutiérrez and Parada, 2010). To simplify the modeling, magma is instantaneously emplaced in a single shoot and further replenishment is not considered (Bea, 2010; Gutierrez and Parada, 2010; Rodriguez et al., 2015). Time step for calculations varies from 15 to 24 years and the grid size used is set at 100 m. The initial temperature distribution of the crust is delimited for the imposed geothermal gradient. Lateral walls of the country rock are considered as insulators.

Results

We have performed numerical simulations of cooling magma chambers emplaced at different pressures and temperatures according to the assumptions previously described. We used horizontal thermal profiles at 11 and 14.4 km of depth, depending on the pressure of emplacement, to delimit the distance over which the host is above the temperature of partial melting and cordiertite stabilization. The beginning of the crustal partial melting is estimated to start above 635 ºC for 3 kbar of pressure and 650 ºC for 4 kbar of pressure (Spear, 1994). These temperatures will be taken as reference to study the zone affected by partial melting in thermal profiles from numerical modeling. The Crd stabilization starts at 525 ºC and 560 ºC under pressures of 3 and 4 kbar, respectively (Spear, 1994). The position with respect of magma chamber boundary of both isograde is represented with respect to the time for each case study (Fig. 10a to d). The more extended zone affected by partial melting (≈ 650 m) is found for a totally liquid magma chamber emplaced at 4 kbar (Fig. 10d). In the cases of partially crystallized (X_c = 0.5) and crystal-absent magma chambers emplaced at 3 kbar (Fig. 10a and c, respectively), migmatites are constrained to

538 the first 300 to 400 m from the pluton boundary. The stabilization of Crd according to the reaction
539 Mg-Chl + Als = Mg-Crd (Spear, 1994) is chiefly influenced by the thermal maturity of the host
540 rock, which is related to imposed pressure conditions. For both emplacement temperatures, Crd-
541 aureoles extend above 1200 m in the cases of magma chambers emplaced at 4 kbar (Fig. 10b, d),
542 whereas they are around 700-800 m in 3 kbar models (Fig. 10a, c).
543 The simulation of the instantaneous emplacement of a single magmatic pulse that has the
544 dimensions observed in the Flamenco pluton promotes the formation of a homogeneous aureole
545 around the magma chamber. The expected aureole by the magma intrusion expected for the
546 Flamenco pluton emplacement varies their length scale from 650 m (case study 1) to 1500 m (case
547 study 4) (Fig. 10).
548
549
550 **6.- Discussion**
551
552 *6.1 Geochemical constraints*
553
554 This study has focused on describing the geochemistry of the granitoids that comprise the Flamenco
555 pluton and the interaction between intrusive magmas and the metasedimentary host rocks at the
556 emplacement level. The extent of the observed interaction and the scarcity of voluminous high-
557 grade metamorphic domains in the Paleozoic basement of the Coastal Range batholith allow us to
558 assess the magma emplacement mechanisms that formed the Flamenco pluton in the Jurassic-
559 Cretaceous magmatic arc in the western margin of South America.
560 In its northern area, the Flamenco pluton granitoids belong to a calcic, magnesian and
561 metaluminous series, with wide geochemical variability, from gabbros to granodiorites, typical of
562 syn-collisional volcanic arc settings (Fig. 4). Sample plots show a linear evolution trend,
563 characteristic of magmatic fractionation processes (Fig. 5, 7). These diagrams show a clear
564 compositional affinity between Flamenco samples and calc-alkaline cordilleran batholiths. These
565 patterns are referred to as cotectic lines of liquids (CLL; Castro, 2013), representing liquids
566 fractionating from an equilibrium saturating solid assemblage at different temperatures. These
567 mineral assemblages are dominated by Px in the less evolved magmas, with a distribution
568 coefficient (D) <1 for all REEs, and Hbl in granodiorites, in which D is >1 for the HREE, producing
569 steeper REE patterns (Fig. 7e), and possibly accompanied by Pl, which is characteristic of calc-
570 alkaline systems. Qtz-diorites and tonalites coincide with primary andesitic magma fields and are
571 genetically related to typical compositions of evolved andesites (Green, 1982; Kelemen et al., 2003)

572 (Fig. 8), whereas granodiorites evolve along cotectic experimental lines drawn by liquids developed
573 at undersaturated and low-pressure conditions (Fig. 6). The preponderance of sharp contacts and the
574 absence of gradual transition between granitoid bodies suggest that differentiation processes from
575 Qtz-diorites to granodiorites do not occur in-situ at the emplacement level. Cotectic trends plotted
576 from the Flamenco samples are consistent with the compositional fields of huge paradigmatic
577 cordilleran batholiths (Peninsular Range: Lee et al., 2007; Patagonia: Hervé et al., 2007; Pankhrust
578 et al., 1999); and available geochemical data indicates that other Coastal Cordillera batholiths are
579 spatially and temporally related to the Flamenco pluton (Copiapó Plutonic Complex: Marschik et
580 al., 2003; and Limarí-Papudo-Illapel batholith: Parada et al., 1999) (Fig. 5, 6 and 7).
581 Some field relations and variations in the geochemical trends described here are representative of
582 the interaction between the intrusive magma and the metasedimentary host rocks. According to
583 petrographic descriptions, the presence in some granodiritic facies (NM-2) of large prismatic
584 euhedral pinnite-biotite crystals, typical of Crd pseudomorphs (Fig. 2f), as well as polycrystalline
585 Qtz xenocrysts are related to assimilation processes. The peritectic euhedral Crd crystallizes in
586 magmatic environments where xenolithic pelite melting reactions occur (Erdmann et al., 2007,
587 Diaz-Alvarado et al., 2011). Furthermore, some granodioritic samples are enriched in MgO and
588 alkalis, coupled with an increasing alumina saturation index (Fig 4c, 5). These are traces of local
589 contamination with pelitic country rocks (Díaz-Alvarado et al., 2011; Castro et al., 2014; Bellos et
590 al., 2015). FM-An-Or (Fig. 6) and CaO vs MgO (Fig. 7a) are definite projections to expose and
591 measure the extension of assimilation processes (Díaz-Alvarado et al., 2011). NM-2 and NM-6
592 granodiorites show crossed trends related to fractionation linear arrangements, pointing to pelites
593 and graywackes in the field. Therefore, assimilation processes that involve Flamenco granitoids
594 produce small scale geochemical variations, and further limited to those areas near the contacts.
595 Interaction processes are mostly mechanical, and a short range geochemical assimilation is limited
596 to a few meters along the contact.
597
598 *6.2 Deformational phases and emplacement*
599
600 There is a significant relationship between deformational phases and structures, the space
601 generation, and the emplacement and formation of large batholiths. Thus, the Jurassic-Cretaceous
602 magmatic arc in the Coastal Cordillera in northern Chile provides an exceptional example of
603 magmatism relating the tectonic inversion deformation at a convergent margin that has evolved
604 from extensional tectonics, framed in a retreating subduction boundary context in the Early Jurassic

605 to Early Cretaceous, to compressive tectonics (Williams et al., 1989; Arévalo and Grocott, 1997;
606 Grocott and Taylor, 2002).
607 At the northern contact, the Flamenco pluton is emplaced in a phyllite-quartzite succession with
608 volcano-sedimentary rocks of the Las Tórtolas formation. The study area has been divided into
609 three zones according to their structural characteristics (Fig. 1d). To the west, melange facies show
610 a total dismantling of the original turbidite architecture, presenting a planar-linear fabric and a NW-
611 SE trending main stretching lineation. This deformation has been dated as Late Carboniferous (Bell,
612 1987). Similar orientations are observed in the stretching lineations marked by granoblastic Crd in
613 the contact aureole (Fig. 2d), but framed by contact metamorphism during the Early Jurassic
614 intrusive process. This extensional deformation phase could be syn-tectonic with boudinage
615 structures described in the volcanic rocks of the study area (Fig. 2b), and coincides with crustal-
616 scale N-S to NWN-SES trending detachments, with top to east kinematics that determine the main
617 emplacement episode (D2 phase, Grocott and Taylor, 2002). Additionally, this is consistent with the
618 main NW-SE orientation of the tabular intrusive sheets that form the Flamenco pluton (Grocott and
619 Wilson, 1997). Grocott and Taylor (2002) described the subsequent D3 and D4 phases as a result of
620 the roof uplift and pluton filling with high emplacement rates related to space generation. The
621 presence of straight or slightly inclined folds and steeped foliations and lineations measured
622 throughout the study area correlate with these deformational phases. Syn-emplacement structures
623 fold the Crd-schists that belong to the contact aureole generated during the early intrusive phases.
624 Thrust faults and associated propagation folds in the east of the study area that promote the auto-
625 thrusting of boudin blocks crosscut the previous structures. There is no precise dating of these
626 structures, and they may develop during horizontal flattening proposed for the late emplacement
627 process (Grocott and Taylor, 2002) or during the crustal scale tectonic compressive phase at the
628 continental margin.
629
630 *6.3 Self-granulitization and thermal aureole*
631
632 According to the assemblage of various geochemically distinguishable granitic facies and to the
633 variety of structures generated during pluton building, the Flamenco pluton was formed during a
634 protracted emplacement process. Qtz-dioritic and granodioritic magmatic facies (NM-3 and NM-6
635 samples) described in the northern margin of the pluton show granulitization textures and
636 temperatures, acquired during the successive intrusion of magmatic pulses. Temperatures of 780 ±
637 10 °C recorded by granoblastic Hbl-Pl equilibriums (Fig. 9) represent the response of previously
638 emplaced granitoids to the thermal input of subsequent intrusive stages. In this sense, self-

639 granulitization and the observed sharp contacts between the different magmatic facies suggest that
640 the first pulses are close to or below its *solidus* temperature during sucessive intrusive phases. This
641 may also be caused by the thermal immaturity of the crust in the early stages of the pluton building.
642 The hypothesis of the sequential emplacement for the formation of Flamenco pluton, and the
643 scarcity of extensive high-grade domains in the fertile metasedimentary host rocks of the Coastal
644 Range batholith, have been contrasted with the 2D thermo-numerical model of a magma chamber
645 with similar dimensions to the Flamenco pluton (Fig. 10). Therefore, it has been possible to
646 compare the development of the observed thermal aureole and that calculated by the thermal
647 modeling. Firstly, the thermal aureole predicted by the 2D model show a homogeneous shape and
648 development around the pluton, whereas the observed aureole presents further development to the
649 south, and a very irregular shape in the north area of the Flamenco pluton (Fig. 10e). The proposed
650 emplacement temperatures for the case studies are between 992 and 1159 °C for intrusive magmas
651 (Table 3), far above the minimum temperature yield by the Hbl-Pl thermobarometry (900 °C, Table
652 2). The model results also show the influence of the depth of emplacement for the development of
653 the contact aureole (Table 3, Fig. 10).
654 According to the proposed model, the established temperatures for the melting reactions in the host-
655 rocks can be located at distances between 200 and 650 m from the magma chamber boundary (Fig.
656 10), depending on the fixed initial conditions and for elapsed times of 10^5 years from the magma
657 emplacement. The high-grade conditions are achieved and maintained for longer times in the case
658 study of emplacement at liquidus temperatures and 4 kbar. However, the south contact of the
659 Flamenco pluton presents a noteworthy domain of migmatitic rocks (distances from the pluton
660 contact up to 2 Km, Grocott and Taylor, 2002), as in the north contact, in spite of presenting
661 tectonic contacs, migmatite outcrops are scarce and Crd-schists are limited to, at most, the first
662 kilometer from the contact (Fig. 10e). Thus, the irregular development of the contact aureole
663 observed in the Flamenco pluton, in comparison with that obtained by thermo-numerical modeling,
664 together with the self-granulitization processes described in marginal magmatic facies in the north
665 area, point to a sequential building for the pluton. To explain this irregularity of the contact aureole
666 and the presence of large migmatitic domains in the south, it is necessary to invoke an intrusive
667 complex growth by accretion from north to south (in its current location), allowing the high-grade
668 aureole development of the host rocks in this area.
669
670
671 **7.- Concluding remarks**
672

673 The descriptions of granitoids with granulitic textures in the pluton margins and the contact
674 metamorphism aureoles point to the conditions in which the Flamenco pluton has been built. Thus,
675 in the framework of the theoretical limits established by the simple 2D thermal modeling approach,
676 we find first-order constraints on the thermal response of the host crust, and setting the
677 emplacement mechanisms of intrusive magmas. Therefore, the processes of self-granulitization and
678 the irregular contact aureole described in this paper indicate that the Flamenco pluton is formed by a
679 protrated process of repeated intrusion of magma pulses, as is pointed by the presence of folded
680 aureole rocks. The successive emplacement is preferably located over previous granitoid batches.
681 Otherwise, the accumulation of intrusive pulses in the crust would generate a higher thermal
682 maturity in the host-rocks, although this also has been shown to be related to emplacement rates,
683 and would increase the interaction processes between granitic melts and metasediments.
684
685
686 **Acknowledgments**
687
688 This work has been developed during the PhD Thesis proposal of Natalia Rodríguez, carried out at
689 the Department of Geology of the University of Atacama. The work was funded with FONDECYT
690 Project Nº 11140722 of CONICYT, and with the fund support of DIUDA 2013-22268 and DIUDA
691 2014-22273 projects. We are grateful for constructive colleague reviews by Gustavo Miranda and
692 Wolfgang Griem, all of which improved the manuscript.
693
694
695 **References**
696
697 Aguirre, L., Herve, F., Godoy, E., 1972. Distribution of metamorphic facies in Chile, an outline.
698 Kristalinikum 9, 7–19.
699
700 Annen, C., Sparks, R.S.J., 2002. Effects of repetitive emplacement of basaltic intrusions on thermal
701 evolution and melt generation in the crust. Earth and Planetary Science Letters 203, 937-955.
702
703 Annen, C., Scaillet, B., Sparks, R.S.J., 2006. Thermal constraints on the emplacement rate of a large
704 intrusive complex: the Manaslu leucogranite, Nepal Himalaya. Journal of Petrology 47, 71–95.
705

706 Annen, C., 2009. From plutons to magma chambers: Thermal constraints on the accumulation of
707 eruptible silicic magma in the upper crust. Earth and Planetary Science Letters 284(3-4), 409-416.
708
709 Annen, C., 2011. Implications of incremental emplacement of magma bodies for magma
710 differentiation, termal aureole dimensions and plutonism-volcanism relationships. Tectonophysics
711 500, 3-10.
712
713 Bachmann, O., Bergantz, G.W., 2004. On the origin of crysytal-poor rhyolites: extracted from
714 batholitic crystal mushes. Journal of Petrology 45, 1565-1582.
715
716 Bahlburg, H., Breitkreutz, C., Zeil, W., 1986. Paläozoische Sedimente Nordchiles. Berliner
717 Geowissenschaftliche Abhandlungen, Reihe A 66, 147-168.
718
719 Bea, F., 2010. Crystallization dynamics of granite magma chambers in the absence of regional
720 stress: Multiphysics modeling with natural examples. Journal of Petrology 51, 1541-1569.
721
722 Beard, J.S., Ragland, P.C., Crawford, M.L., 2005. Reactive bulk assimilation: a model for the crust-
723 mantle mixing in silicic magmas. Geology 33, 681–684.
724
725 Bell, C.M., 1982. The Lower Paleozoic metasedimentary basement of the coastal range of Chile
726 between 25°30' and 27°S. Revista Geológica de Chile 9 (3), 21-29.
727
728 Bell, C.M., 1987. The origin of the Upper Paleozoic Chañaral mélange of N Chile. Journal of the
729 Geological Society of London 144, 599-610.
730
731 Bellos, L.I., Castro, A., Díaz-Alvarado, J., Toselli, A., 2015. Multi-pulse cotectic evolution and in-
732 situ fractionation of calc-alkaline tonalite–granodiorite rocks, Sierra de Velasco batholith,
733 Famatinian belt, Argentina. Gondwana Research 27, 258-280.
734
735 Berg, K., Breitkreuz, C., 1983. Mesozoische Plutone in der nordchilenischen Küstenkordillere:
736 Petrogenese, Geochronologie, Geochemie und Geodynamik mentelbetonter Magmatite.
737 Geotektonische Forschungen 66, 107 p.
738

739 Berg, K., Breitkreuz, C., Damm, K.W., Pichowiak, S., Zeil, W., 1983. The North-Chilean Coast
740 Range - an example for the development of an active continental margin. Geologische Rundschau
741 72, 715–731.
742
743 Berg, K., Baumann, A., 1985. Plutonic and metasedimentary rocks from the Coastal range of
744 northern Chile. Rb-Sr and U-Pb isotope systematics. Earth and Planetary Sciences Letters 75, 101–
745 115.
746
747 Bohrson,W.A., Spera, F.J., 2001. Energy-constrained open system magmatic processes II:
748 application of energy-constrained assimilation-fractional crystallization (EC-AFC) model to
749 magmatic systems. Journal of Petrology 42 (5), 1019–1041.
750
751 Brook, M., Pankhurst, R., Sheperd, T., Spiro, B., Snelling, N., Swainbank, I., 1986. Andean
752 geochronology and metallogenesis. Overseas Development Administration, Open File Report, 83
753 p., London.
754
755 Burgisser, A., Bergantz, C.W., 2011. A rapid mechanism to remobilize and homogenize highly
756 crystalline magma bodies. Nature 471, 212–215.
757
758 Castro, A., 2013. Tonalite–granodiorite suites as cotectic systems: a review of experimental studies
759 with application to granitoid petrogenesis. Earth-Science Reviews 124, 68-95.
760
761 Castro, A., Díaz-Alvarado, J., Fernández, C., 2014. Fractionation and incipient self-granulitization
762 during deep-crust emplacement of Lower Ordovician Valle Fértil batholith at the Gondwana active
763 margin of South America. Gondwana Research 25, 685-706.
764
765 Castro, A., 2014. The off-crust origin of granite batholiths. Geoscience Frontiers 5, 63-75.
766
767 Chapman, D.S., Furlong, K.P., 1992. Thermal state of the continental lower crust. Elsevier,
768 Amsterdam.
769
770 Charrier, R., Pinto, L., Rodríguez, M.P., 2007. Tectonostratigraphic evolution of the Andean
771 Orogen in Chile. In: T. Moreno and W. Gibbons (eds.). The Geology of Chile, The Geological
772 Society, Londres, pp. 21–114.

773
774 Clemens, J.D., Stevens, G., Farina, F., 2011. The enigmatic sources of I-type granites: the peritectic
775 connexion. Lithos 126 (3–4), 174–181.
776
777 Clemens, J.D., Stevens, G., 2012. What controls chemical variation in granitic magmas? Lithos
778 134–135, 317–329.
779
780 Condie, K.C., 1998. Episodic continental growth and supercontinents: a mantle avalanche
781 connection? Earth Planetary Science Letters 163, 97-108.
782
783 Condie, K.C., 2000. Episodic continental growth models: afterthoughts and extensions.
784 Tectonophysics 322, 153-162.
785
786 Coleman, D.S., Gray,W., Glazner, A.F., 2004. Rethinking the emplacement and evolution of zoned
787 plutons: geochronologic evidence for incremental assembly of the Tuolumne Intrusive Suite,
788 California. Geology 32, 433–436.
789
790 Dallmeyer, R.D., Brown, M., Grocott, J., Taylor, G.K., Treloar., P.J., 1996. Mesozoic Magmatic
791 and Tectonics Events within the Andean Plate Boundary Zone, 26°-27°30'S, North Chile:
792 Constraints from 40Ar/39Ar Mineral Ages. The Journal of Geology 104 (1), 19-40.
793
794 de Silva, S.L., Gregg, P.M., 2014. Thermomechanical feedbacks in magmatic systems: Implications
795 for growth, longevity, and evolution of large caldera-forming magma reservoirs and their
796 supereruptions. Journal of Volcanology and Geothermal Research 282, 77-91.
797
798 Díaz, F., 1986. Hoja Salvador, borradores de terreno (Inédito). Servicio Nacional de
799 Geología y Minería, Santiago.
800
801 Díaz Alvarado, J., Castro, A., Fernández, C., Moreno-Ventas, I., 2011. Assessing bulk assimilation
802 in cordierite-bearing granitoids from the Central System batholith, Spain; experimental,
803 geochemical and geochronological constraints. Journal of Petrology 52, 223–256.
804

805 Díaz Alvarado, J., Fernández, C., Díaz Azpiroz, M., Castro, A., Moreno-Ventas, I., 2012. Fabric
806 evidence for granodiorite emplacement with extensional shear zones in the Variscan Gredos massif
807 (Spanish Central System). Journal of Structural Geology 42, 74–90.
808
809 Díaz-Alvarado, J., Castro, A., Fernández, C., Moreno-Ventas, I., 2013. SHRIMP U–Pb zircon
810 geochronology and thermalmodeling of multilayer granitoid intrusions. Implications for the
811 building and thermal evolution of the Central System batholith, Iberian Massif, Spain. Lithos 175–
812 176, 104–123.
813
814 Dufek, J., Bergantz, G.W., 2005. Lower Crustal Magma Genesis and Preservation: a Stochastic
815 Framework for the Evaluation of Basalt–Crust Interaction. Journal of Petrology 46(11), 2167-2195.
816
817 Farrar, E., Clark, A., Haynes, J., Quirt, G., Conn, H., Zentilli, M., 1970. K-Ar evidence for the post-
818 Paleozoic migration of granitic intrusion foci in the Andes of northern Chile. Earth and Planetary
819 Science Letters. Vol. 10, p. 60-66.
820
821 Frost, B.R., Barnes, C.G., Collins,W.J., Arculus, R.J., Ellis, D.J., Frost, C.D., 2001. A geochemical
822 classification for granitic rocks. Journal of Petrology 42, 2033-2048.
823
824 Gelman, S.E., Gutierrez, F.J., Bachmann, O., 2013. On the longevity of large upper crustal silicic
825 magma chambers. Geology 41, 759-762.
826
827 Gelman, S.E., Deering, C.D., Bachmann, O., Huber, C., Gutiérrez, F.J., 2014. Identifying the
828 crystal graveyards remaining after large silicic eruptions. Earth and Planetary Science Letters 403,
829 299-306.
830
831 Glazner, A.F., Bartley, J.M., Coleman, D.S., Gray, W., Taylor, R.Z., 2004. Are plutons assembled
832 over millions of years by amalgamation from small magma chambers. GSA Today 14, 4–11.
833
834 Godoy, E., 1997. El Gabro Orbicular de Quebrada Animas Viejas, provincia de Chañaral, Chile. In
835 Congreso Geológico Chileno No. 8, Actas, 2, pp. 1285-1289, Antofagasta.
836
837 Godoy, E., Lara, L., 1998. Hojas Chañaral y Diego de Almagro. Servicio Nacional de Geología y
838 Minería, Mapas Geológicos, 5-6 (1:100.000), Santiago.

González, G., Scheuber, E., 1997. La tectónica del arco magmático del Jurásico-Cretácico Inferior, Cordillera de la Costa (22-26°S), Norte de Chile: Una historia de Deformación cortical en un límite de placas convergentes. Proceedings 7th. Congreso Geológico Chileno, Universidad Católica del Norte, Antofagasta (Chile).

Grocott, J., Brown, M., Dallmeyer, R.D., Taylor, G.K., Treloar, P.J., 1994. Mechanism of continental growth in extensional arcs: An example from de Andean plate-boundary zone. Geology 22, 391–394.

Grocott, J., Taylor, G.K., 2002. Magmatic arc fault systems, deformation partitioning and emplacement of granitic complexes en the Coastal Cordillera, north Chilean Andes (25°30'S to 27°30'S). Journal of the Geological Society of London 159, 425-442.

Gualda, G.A.R., Ghiorso, M.S., Lemons, R.V., Carley, T.L., 2012. Rhyolite-MELTS: a Modified Calibration of MELTS Optimized for Silica-rich, Fluid-bearing Magmatic Systems. Journal of Petrology 53, 875-890.

Gutiérrez, F., Parada, M.A., 2010. Numerical Modeling of Time-dependent Fluid Dynamics and Differentiation of a Shallow Basaltic Magma Chamber. Journal of Petrology 51, 731-762.

Herve, F., Pankhurst, R.J., Fanning, C.M., Calderon, M., Yaxley, G.M., 2007. The South Patagonian batholith: 150 my of granite magmatism on a plate margin. Lithos 97, 373-394.

Holland, T., Blundy, J., 1994. Non-ideal interactions in calcic amphiboles and their bearing on amphibole-plagioclase thermometry. Contrib Mineral Petrol 116, 433-447.

Huber, C., Bachmann, O., Manga, M., 2009. Homogenization processes in silicic magma chambers by stirring and mushification (latent heat buffering). Earth and planetary science letters 283, 38-47.

Huppert, H.E., Sparks, S.J., 1988. The generation of granitic magma by intrusion of basalt into continental crust. Journal of Petrology 29 (3), 599–624.

872 Kemp, A.I.S., Hawkesworth., 2003. Granitic perspectives on the generation and secular evolution of
873 the continental crust. In: Holland, H.D., Turekian, K.K., Rudnick, R.L. (Eds.), The Crust. Treatise
874 on Geochemistry, Vol. 3. Elsevier Pergamon, Oxford, pp. 349-410.
875
876 Koyaguchi, T., Kaneko, K., 2000. Thermal evolution of silicic magma chambers after basalt
877 replenishment. Transactions of the Royal Society of Edimburgh 91, 47-60.
878
879 Kretz, R., 1983. Symbols for rock-forming minerals. American Mineralogist 68, 277-279.
880
881 Le Breton, N., Thompson, A.B., 1988. Fluid-absent (dehydration) melting of biotite in metapelites
882 in the early stages of crustal anatexis. Contributions to Mineralogy and Petrology 99, 226-237.
883
884 Lee, C.-T.A., Morton, D.M., Kistler, R.W., Baird, A.K., 2007. Petrology and tectonics of
885 Phanerozoic continent formation: from island arcs to accretion and continental arc magmatism.
886 Earth and Planetary Science Letters 263, 370-387.
887
888 Levi, B., Aguirre, L., 1981. Ensialic spreading-subsidence in the Mesozoic and Paleogene of central
889 Chile. Journal of the Geological Society, London 138, 75-81.
890
891 Marschik, R., Fontignie, D., Chiaradia, M., Voldet, P., 2003. Geochemical and Sr-Nd-Pb-O isotope
892 composition of granitoides of the Early Cretaceous Copiapó plutonic complex (27°30´S), Chile.
893 Journal of South American Earth Sciences 16, 381-398.
894
895 Menand, T., Daniels, K., Benghiat, P., 2010. Dyke propagation and sill formation in a compressive
896 tectonic environment. J. Geophys. Res. 115, 1-12.
897
898 Menand, T., Annen, C., Saint Blanquat, M., 2015. Rates of magma transfer in the crust: Insights
899 into magma reservoir recharge and pluton growth. Geology 43 (3), 199-202.
900
901 Michaut, C., Jaupart, C., 2011. Two models for the formation of magma reservoirs by small
902 increments. Tectonophysis 500, 34-49.
903
904 Miller, H., 1970. Vergleichende Studien an prämesozoischen Gesteinen Chiles unter
905 besonderer Berücksichtigung ihrer Kleintektonik. Geotektonische Forschungen, Vol 36, 64 p.

Miller, J.S., Matzel, J.E.P., Miller, C.F., Burgess S.D., Miller, R.B., 2007. Zircon growth and recycling during the assembly of large, composite arc plutons. Journal of Volcanology and Geothermal Research 167, 282–299.

Molina, P.G., Parada, M.A., Gutiérrez, F.J., Ma, C., Li, J., Yuanyuan, L., Reich, M., Aravena, Á., 2015. Protracted late magmatic stage of the Caleu pluton (central Chile) as a consequence of heat redistribution by diking: Insights from zircon data and thermal modeling. Lithos 227, 255-268.

Mpodozis, C., Kay, S.M., 1990. Provincias magmáticas acidas y evolución tectónica de Gondwana: Andes Chilenos (28-31°S). Revista Geológica de Chile 17 (2), 153-180.

Mpodozis, C., Ramos, V.A., 2008. Tectónica Jurásica en Argentina y Chile: extensión, subducción oblicua, rifting, deriva y colisiones? Revista Asociación Geológica de Argentina, 63 (4), 481-497.

Naranjo, J.A., Puig, A., 1984. Hojas Taltal y Chañaral, regiones de Antofagasta y Atacama, Servicio Nacional de Geología y Minería, Carta Geológica de Chile, No. 62-63, 140 p., 1 mapa escala 1:250.000, Santiago.

Pankhurst, R.J., Weaver, S.D., Hervé, F., Larrondo, P., 1999. Mesozoic-cenozoic evolution of the North Patagonian batholith in Aysen, southern Chile. Journal of the Geological Society 156, 673-694.

Parada, M.A., Nyström, J.O., Levi, B., 1999. Multiple sources for the Coastal Batholith of central Chile (31-34°S) geochemical and Sr-Nd isotopic evidence and tectonic implications. Lithos 46, 504-521.

Paterson, S.R., Okaya, D., Memeti, V., Economos, R., Miller, R.B., 2011. Magma addition and flux calculations of incrementally constructed magma chambers in continental margin arcs: combined field, geochronologic, and thermal modeling studies. Geosphere 7, 1439–1468.

Pearce, J.A., Harris, N.B.W., Tindle, A.G., 1984. Trace element discrimination diagrams for the tectonic interpretation of granitic rocks. Journal of Petrology 25, 956-983.

940 Plank, T., Langmuir, C.H., 1998. The chemical composition of subducting sediment and its
941 consequences for the crust and mantle. Chemical Geology 145, 325-394.
942
943 Ramos, V.A., 1999. Plate tectonic setting of the Andean Cordillera. Episodes 22(3), 183-190.
944
945 Rodríguez, C., Geyer, A., Castro, A., Villaseñor, A., 2015. Natural equivalents of thermal gradient
946 experiments. Journal of Volcanology and Geothermal Research 298, 47-58.
947
948 Saint Blanquat, M., Horsman, E., Habert, G., Morgan, S., Vanderhaeghe, O., Law, R., Tikoff, B.,
949 2011. Multiscale magmatic cyclicity, duration of pluton construction, and the paradoxical
950 relationship between tectonism and plutonism in continental arcs. Tectonophysics 500, 20-33.
951
952 Saito, S., Arima, M., Nakajima, T., 2007. Hybridization of a shallow 'I-type' granitoid pluton and
953 its host migmatite by magma-chamber wall collapse: TheTokuwa pluton, Central Japan. Journal of
954 Petrology 48, 79-111.
955
956 Schmidt, M.W., 1992. Amphibole composition in tonalite as a function of pressure: an experimental
957 calibration of the Al-in-hornblende barometer. Contributions of Mineralogy and Petrology 110,
958 304-10.
959
960 Spear, F.S., 1994. Metamorphic phase equilibria and pressure-temperature-time paths.
961 Mineralogical Society of America Monograph. 799 p.
962
963 Ulriksen, C. 1979. Regional geology, geochronology and metallogeny of the Coastal Cordillera of
964 Chile between 25° 30' y 26°00'S. M.Sc. Thesis (Unpublished), Dalhousie University, 221 p.,
965 Halifax, Canada.
966
967 Vielzeuf, D., Holloway, J.R., 1988. Experimental determination of the fluid-absent melting
968 relations in the pelitic system. Contributions to Mineralogy and Petrology 98, 257-276.
969
970 Vilas, J.F., Valencio, D.A., 1978. Paleomagnetism of South American and African rocks and the
971 age of the South Atlantic. Revista Brasileira de Geociências 8, 3-10.
972

973 Vogt, K., Gerya, T.V., Castro, A., 2012. Crustal growth at active continental margins: numerical
974 modeling. Physics of the Earth and Planetary Interiors 192–193, 1–20.
975
976 Von Huene, R., Scholl, D.W., 1991. Observations at convergent margins concerning sediment
977 subduction, subduction erosion, and the growth of continental crust. Reviews of Geophysics 29,
978 279–316.
979
980 Wohletz, K., Civetta, L., Orsi, G., 1999. Thermal evolution of the Phlegraean magmatic system.
981 Journal of Volcanology and Geothermal Research 91, 381-414.
982
983 Wyllie, P.J., Huang, W.L., Stern, C.R., Maaloe, S., 1976. Granitic magmas: possible and impossible
984 sources, water contents, and crystallization sequences. Canadian Journal of Earth Sciences 13,
985 1007–1019.
986
987 Wyllie, P.J., 1977. From crucibles through subduction to batholiths. In: Saxena, S.K., Bhattacharjia
988 (Eds.), Energetics of Geological Processes. Springer Verlag, pp. 389–433.
989
990
991 **Figure captions**
992
993 **Figure 1. (**a) Major morphological features of the Andean cordillera in Chile (modified from
994 Charrier et al., 2007). (b) Inset showing the outline of part of the Late Triassic-Early Jurassic
995 Coastal Cordillera batholith. (c) Geological sketch of the entire Flamenco pluton based on field
996 observations and satellite images. **(**d) Detailed geological map of the study area at the northwestern
997 contact of the Flamenco pluton. The locations of the samples used in the geochemical study are
998 indicated on the map.
999 **Figure 2**. Field photographs of some outstanding lithological and structural features of the study
1000 area. (a) Tonalites include irregular and partially digested xenoliths in areas near the contacts with
1001 metasedimentary host-rocks. (b) Self-thrusting of volcano-sedimentary layers showing previous
1002 boudinage and pinch and swell structures. (c) Sharp contacts between intrusive granodiorites and
1003 host Crd-Schists. (d) Elongated Crd crystals (black arrow) indicating the NW-SE syn- post-
1004 emplacement preferred orientation (red lines) of ductile structures in the contact aureole. (e)
1005 Orbicular textures found in gabbros from the study area. (f) Biotite-pinnite crystal clots (black
1006 arrows) showing euhedral prismatic shape and homogeneous grain size.

1007 **Figure 3.** Microphotographs showing the main petrographic characteristic of the studied samples.
1008 Most are cross-polarized light images except (g), which is a BSE image. Gabbros (a) present scarce
1009 Opx crystals, which are observed included in Hbl-Pl polycrystalline aggregates or clots derived
1010 from Px reaction in the melt. Qtz-diorites to granodiorites (b, c, d) show a progressive enrichment in
1011 Qtz and Kfs, and the substitution of Hbl by Bt as the mafic phase. Mesocratic granodiorites located
1012 at the north margin of Flamenco pluton (e, f) present granulitic recrystallization textures. Red
1013 arrows point to noteworthy examples of Hbl-Pl-Qtz triple junctions. Poikiloblastic Kfs and Qtz
1014 recrystallization are observed. Crd-granodiorites (g) show rounded and polycrystalline Qtz, and
1015 concentric zoned Pl and Hbl phenocrysts. Hbl present Bt reaction rims. The groundmass is
1016 composed of Qtz + Pl + Bt + Kfs. Crd-schists (h) present leucocratic Qtz-rich bands alternated with
1017 Crd-rich mesocratic domains. Some Qtz-rich bands show Kfs, incipient igneous textures and Bt-Crd
1018 schlierens, typical of migmatitic leucosomes.
1019 **Figure 4.** (a) O'Connor rock classification triangle, (b, c, d) granitoid classification diagrams (Frost
1020 et al., 2001), and (e) Nb-Y tectonic discrimination diagram (Pearce et al., 1984) for the granitoids of
1021 the northern area of the Flamenco pluton. Only granodiorites show slight deviations from
1022 metaluminous and calcic trends defined by the Flamenco samples. In (e): WPG: Within-plate
1023 granite, ORG: Ocean ridge granite, VAR: Volcanic arc granite, Syn-COLG: Syn-collision granite.
1024 **Figure 5.** Major element vs SiO_2 variation diagrams for the intrusive granitoids comprising the
1025 northern area of Flamenco pluton. The Copiapo Plutonic Complex (Marschik et al., 2003) and
1026 Limari-Papudo-Illapel batholith (Parada et al., 1999) are used as references for chronologically
1027 related plutonic rocks in the Coastal Cordillera batholith. Paradigmatic Cordilleran granitoids are
1028 plotted for comparison (Patagonia batholith: Hervé et al., 2007; Pankhurst et al., 1999; and
1029 Peninsular Range batholith: Lee et al., 2007).
1030 **Figure 6.** Projection of the Flamenco granitoids into the F–An–Or projected space. Cotectic
1031 relations and crossed trayectories are evidenced in the pseudoternary system defined by Opx-An-Or.
1032 The main compositional areas and the experimental granitic evolutions are indicated (Díaz-
1033 Alvarado et al., 2011; Castro, 2013 and references therein). See text for further details.
1034 **Figure 7.** Major and trace element geochemical variations. (a, b, c, d) Fractionation, cotectic-like
1035 and assimilation trends are indicated. Assimilation trajectories point to the host graywackes and
1036 pelites, showing Al_2O_3, FeO and MgO enrichment during CaO depletion. (e) Lu* vs La*/Lu* ratio.
1037 Low HREE values for granodiorites indicate the presence of Hbl during fractionation.
1038 **Figure 8.** Thompson normalization plot rock/MORB for (a) gabbros, Qtz-diorites and tonalites, and
1039 (b) granodiorites. The black line with white squares is the typical continental arc andesite
1040 composition given by Kelemen et al. (2003).

Figure 9. (a) Detailed geological sketch of the Flamenco north contact with the location of samples selected for the thermobarometric study. (b, c, d) BSE images of NA-2 and NM-3 Qtz-dioritic samples. (e, f) BSE images of the NA-6 granodioritic sample. Microprobe analysis points (Table 2) are indicated with representative results of the Hbl-Pl thermobarometry.

Figure 10. (a-d) Thermal modeling results for different case studies. The position of both partial melting and Crd-in isograde are represented according to the time elapsed from the magma chamber emplacement for all case studies. Result for magma chambers emplaced at temperatures equivalent to 0.5 of crystal fraction are given in a (T = 992ºC) and b (T = 1007ºC). The isograde resulting from the emplacement at liquidus temperature are showed in c (T=1141.6ºC) and d (T = 1159ºC) (Table 3). (e) Geological sketch summarizing the main characteristics of the thermal aureole observed in Flamenco pluton. North aureole has been mapped according to the field observations carried out in this study, whereas the south aureole was drawn following the metamorphic aureole described by Grocott and Taylor, 2002.

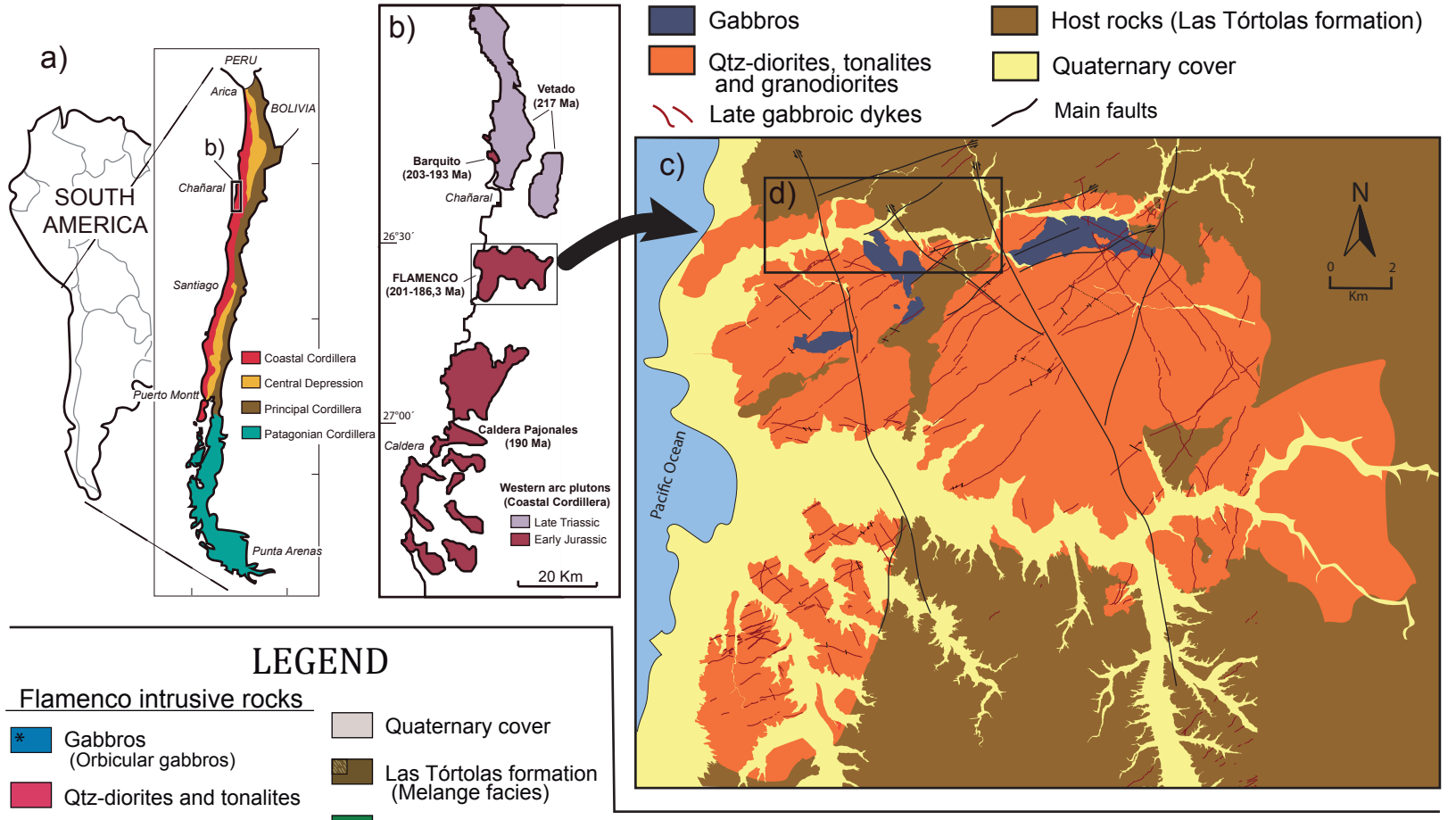

LEGEND

Flamenco intrusive rocks

- Gabbros (Orbicular gabbros)
- Qtz-diorites and tonalites
- Mesocratic granodiorites
- Leucocratic granodiorites (Crd-granodiorites)
- Geochemical samples

- Transcurrent faults
- Thrust faults
- Primary foliation (S_0)
- Tectonic foliation (S_1)
- Fold axial traces

- Quaternary cover
- Las Tórtolas formation (Melange facies)
- Volcano-sedimentary unit
- Contact metamorphism aureole
- Migmatitic hornfelses and Crd-schist
- Late gabbroic dykes

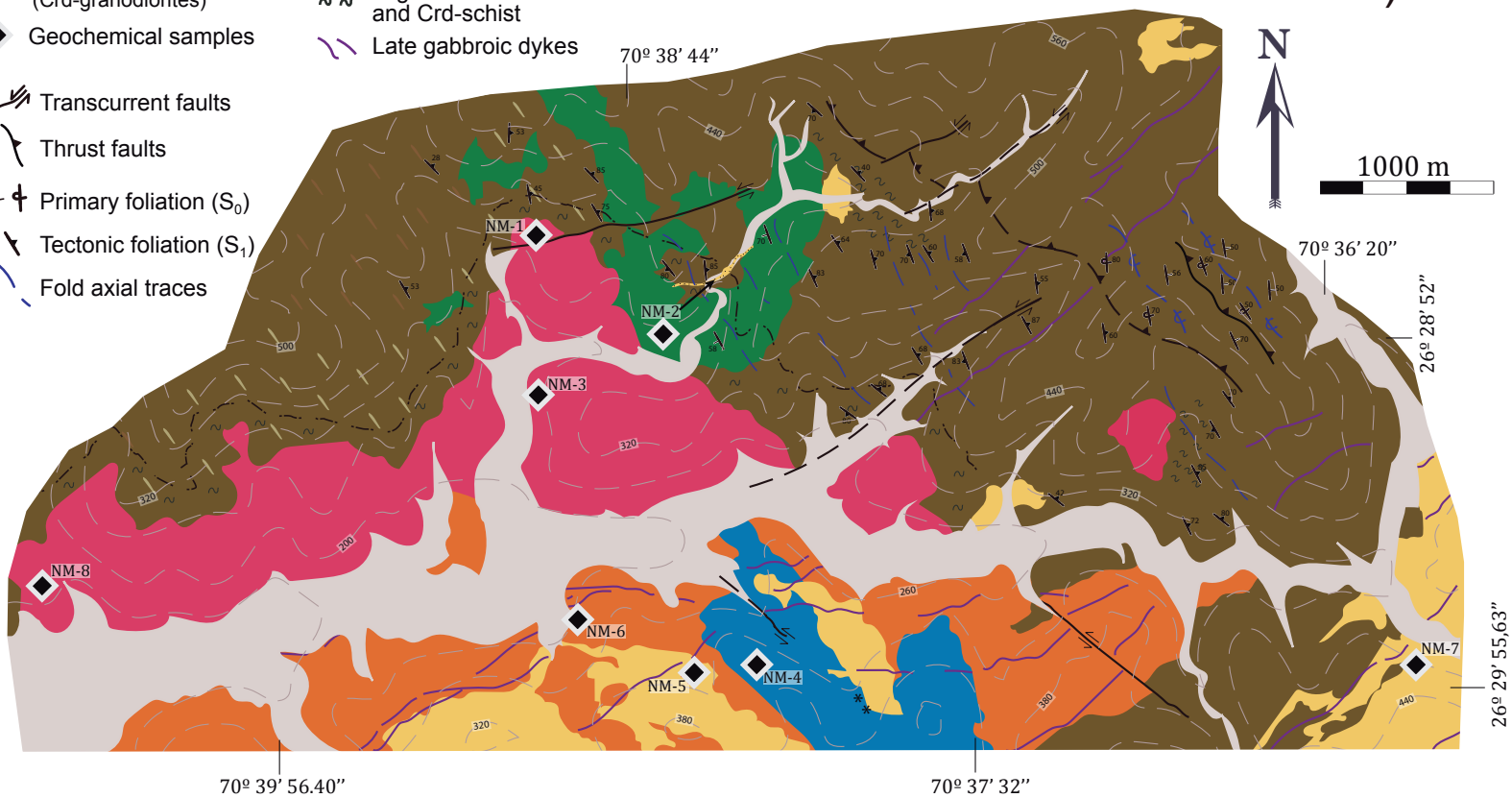


a)
b)
c)
d)
e)
f)

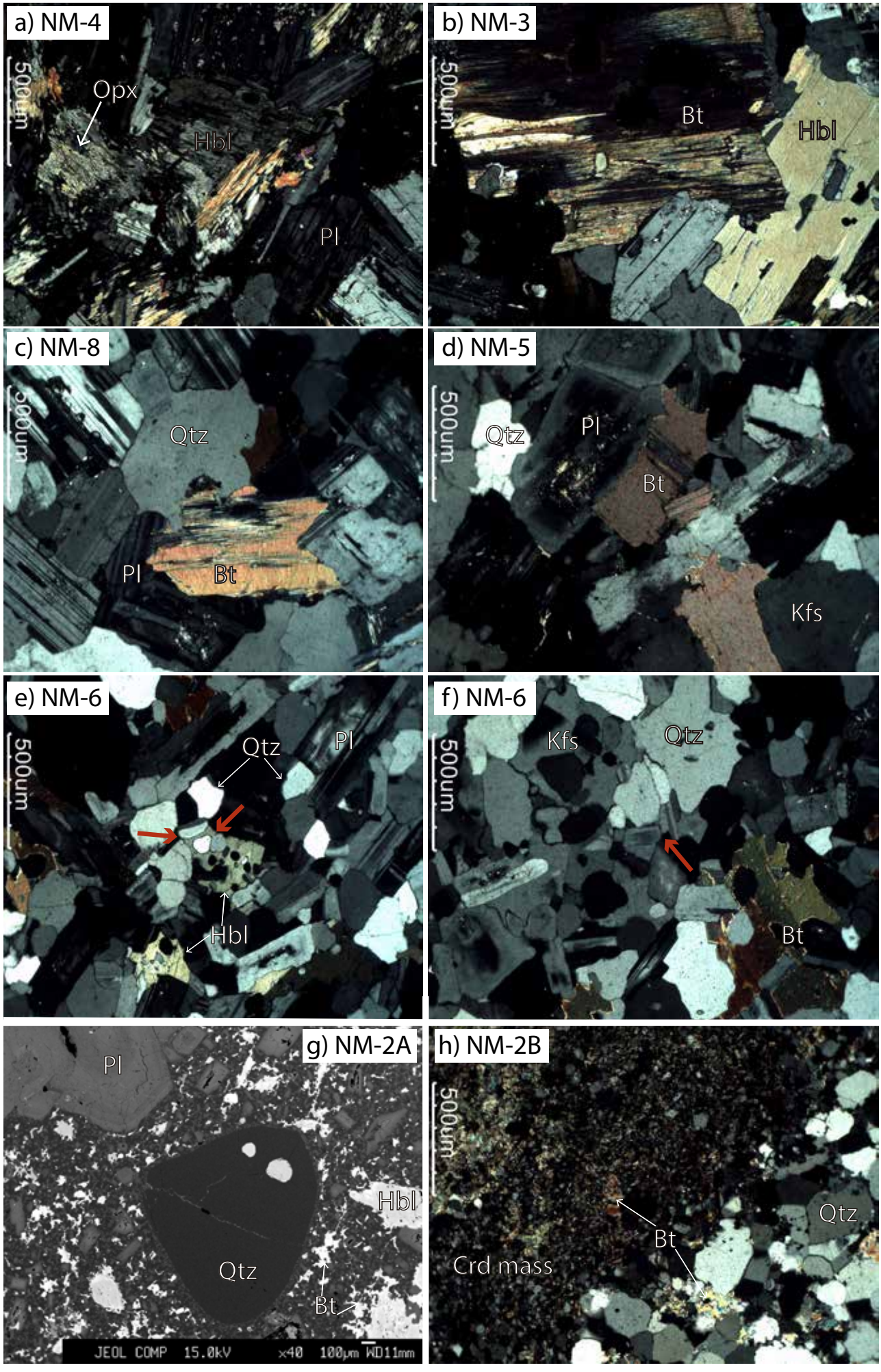
a) NM-4
500um
Opx
Hbl
Pl
b) NM-3
500um
Bt
Hbl
c) NM-8
500um
Qtz
Pl
Bt
d) NM-5
500um
Qtz
Pl
Bt
Kfs
e) NM-6
500um
Qtz
Pl
Hbl
f) NM-6
500um
Kfs
Qtz
Bt
g) NM-2A
Pl
Hbl
Qtz
Bt
JEOL COMP 15.0kV ×40 100μm WD11mm
h) NM-2B
500um
Qtz
Bt
Crd mass

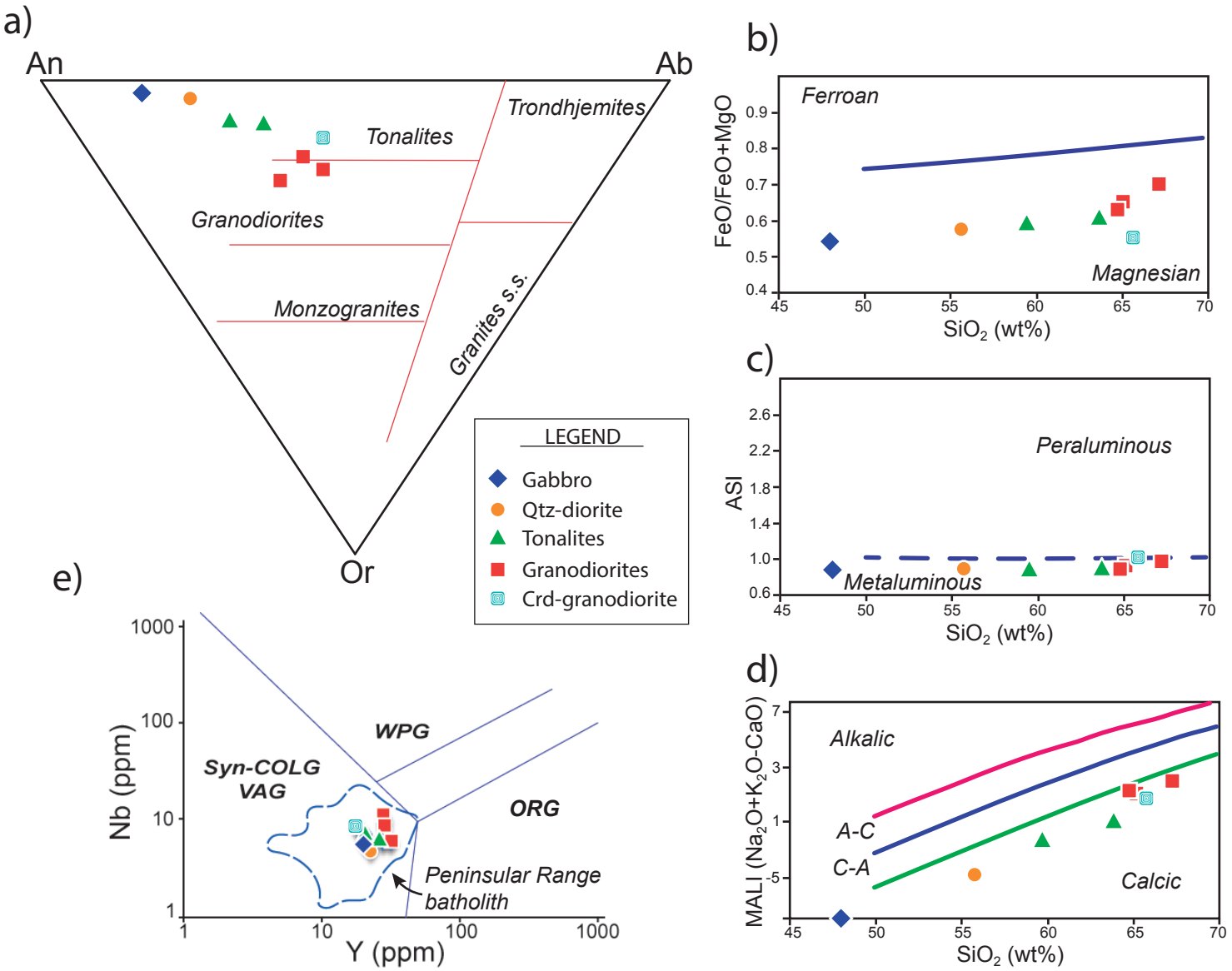
a)
An
Ab
Or
Trondhjemites
Tonalites
Granodiorites
Monzogranites
Granites s.s.
LEGEND
Gabbro
Qtz-diorite
Tonalites
Granodiorites
Crd-granodiorite
b)
Ferroan
Magnesian
FeO/FeO+MgO
SiO2 (wt%)
c)
Peraluminous
Metaluminous
ASI
SiO2 (wt%)
d)
Alkalic
A-C
C-A
Calcic
MALI (Na2O+K2O-CaO)
SiO2 (wt%)
e)
WPG
Syn-COLG
VAG
ORG
Peninsular Range
batholith
Nb (ppm)
Y (ppm)

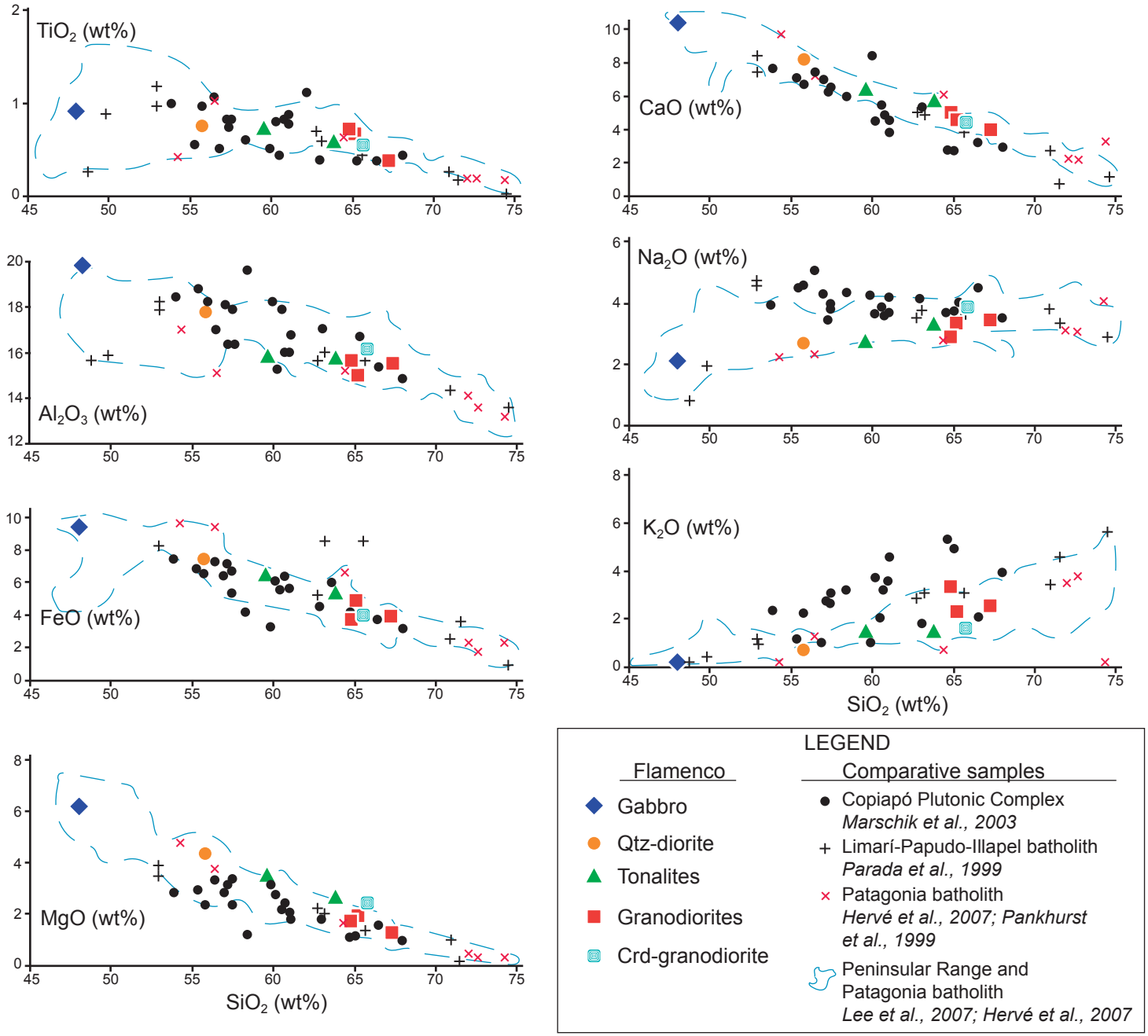
TiO2 (wt%)
CaO (wt%)
Al2O3 (wt%)
Na2O (wt%)
FeO (wt%)
K2O (wt%)
MgO (wt%)
SiO2 (wt%)
SiO2 (wt%)
LEGEND
Flamenco
Gabbro
Qtz-diorite
Tonalites
Granodiorites
Crd-granodiorite
Comparative samples
Copiapó Plutonic Complex
Marschik et al., 2003
Limarí-Papudo-Illapel batholith
Parada et al., 1999
Patagonia batholith
Hervé et al., 2007; Pankhurst et al., 1999
Peninsular Range and Patagonia batholith
Lee et al., 2007; Hervé et al., 2007

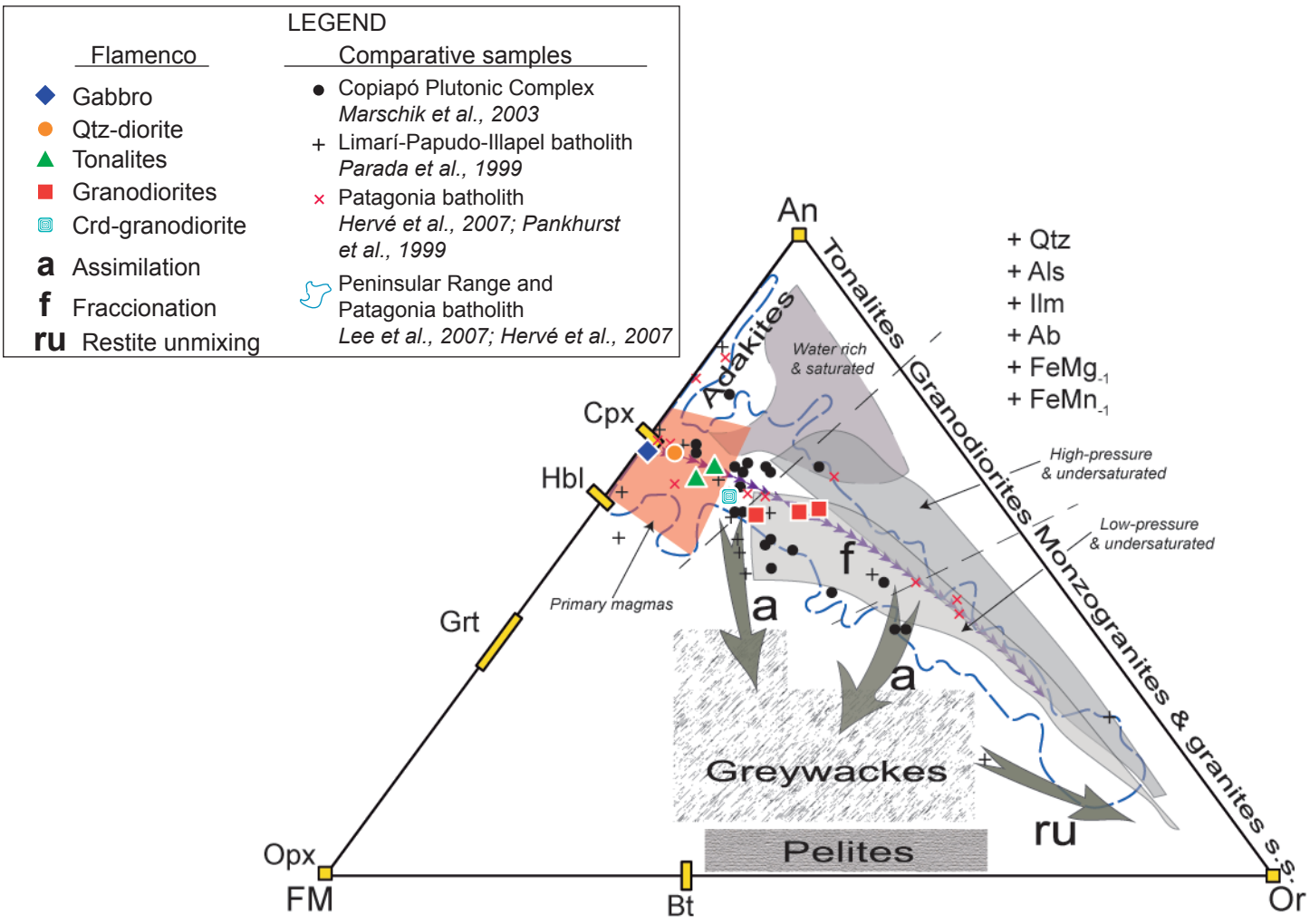
LEGEND
Flamenco
Gabbro
Qtz-diorite
Tonalites
Granodiorites
Crd-granodiorite
a Assimilation
f Fraccionation
ru Restite unmixing
Comparative samples
Copiapó Plutonic Complex
Marschik et al., 2003
Limarí-Papudo-Illapel batholith
Parada et al., 1999
Patagonia batholith
Hervé et al., 2007; Pankhurst et al., 1999
Peninsular Range and Patagonia batholith
Lee et al., 2007; Hervé et al., 2007
An
Tonalites
Granodiorites
Monzogranites & granites s.s.
+ Qtz
+ Als
+ Ilm
+ Ab
+ FeMg-1
+ FeMn-1
Adakites
Water rich & saturated
High-pressure & undersaturated
Low-pressure & undersaturated
Cpx
Hbl
Grt
Primary magmas
f
a
a
Greywackes
Pelites
ru
Opx
FM
Bt
Or

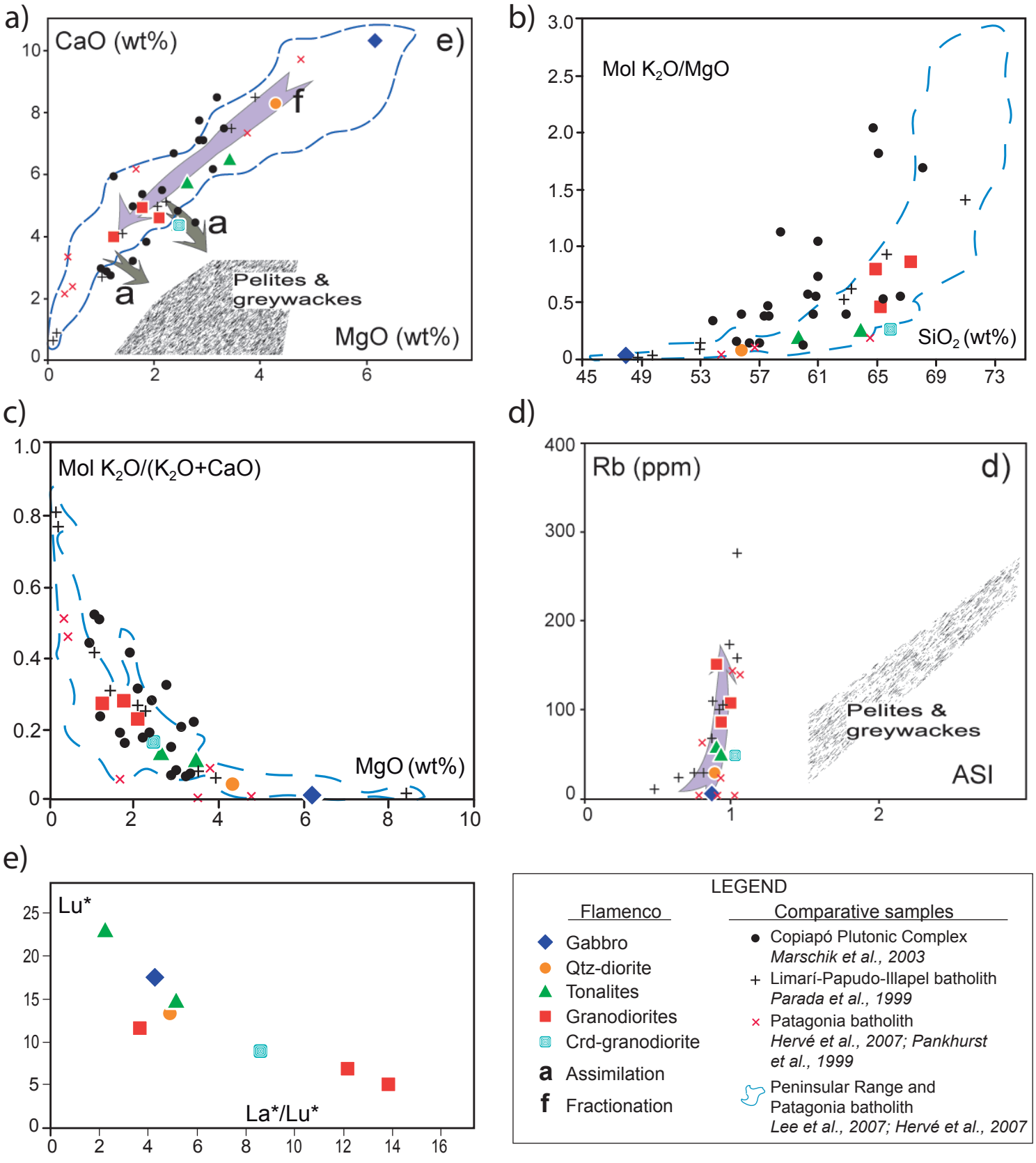
a)
CaO (wt%)
e)
f
a
a
Pelites &
greywackes
MgO (wt%)
b)
Mol K2O/MgO
SiO2 (wt%)
c)
Mol K2O/(K2O+CaO)
MgO (wt%)
d)
Rb (ppm)
d)
Pelites &
greywackes
ASI
e)
Lu*
La*/Lu*
LEGEND
Flamenco
Gabbro
Qtz-diorite
Tonalites
Granodiorites
Crd-granodiorite
a Assimilation
f Fractionation
Comparative samples
Copiapó Plutonic Complex
Marschik et al., 2003
Limarí-Papudo-Illapel batholith
Parada et al., 1999
Patagonia batholith
Hervé et al., 2007; Pankhurst
et al., 1999
Peninsular Range and
Patagonia batholith
Lee et al., 2007; Hervé et al., 2007

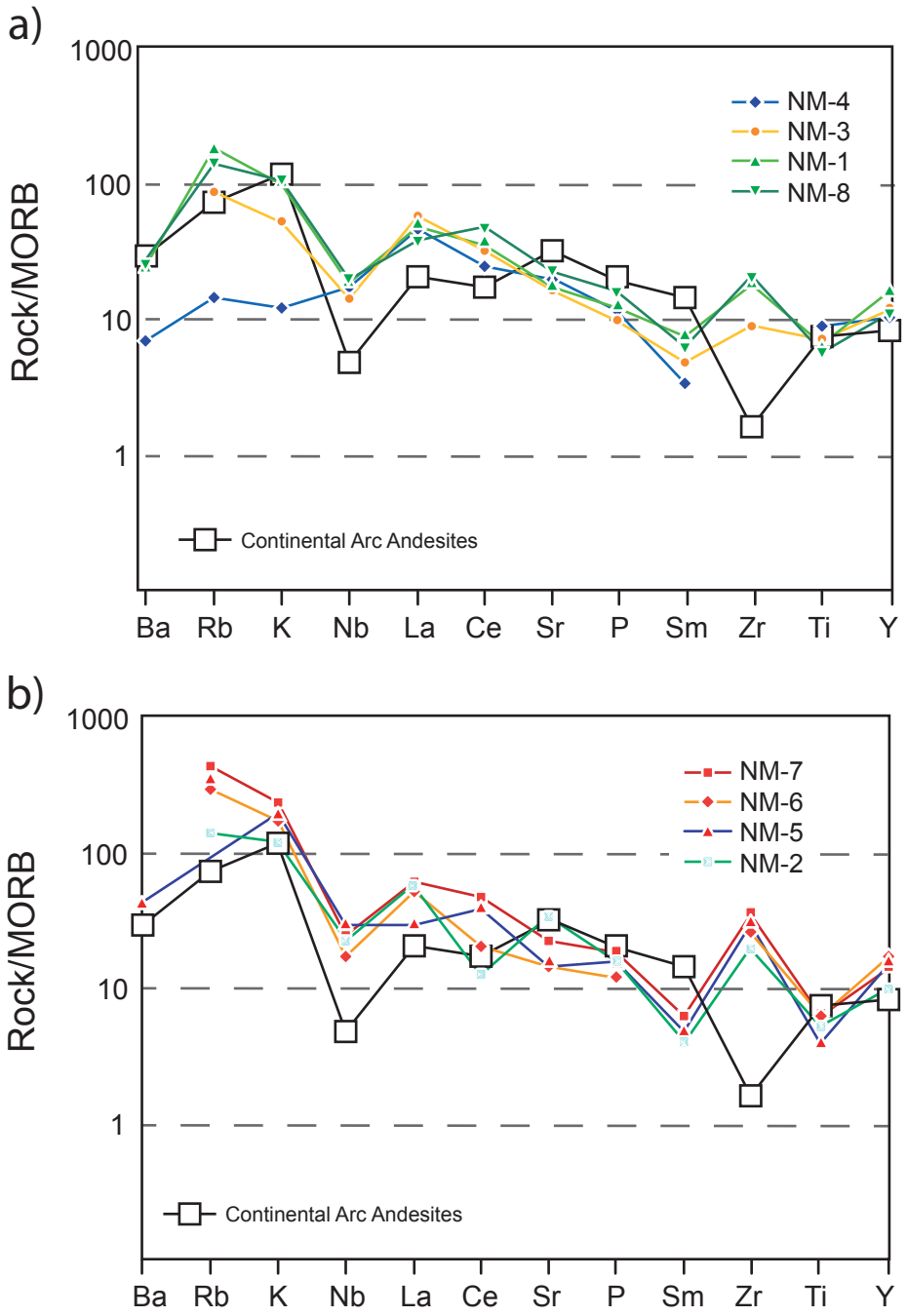
a)
1000
100
10
1
Rock/MORB
NM-4
NM-3
NM-1
NM-8
Continental Arc Andesites
Ba
Rb
K
Nb
La
Ce
Sr
P
Sm
Zr
Ti
Y
b)
1000
100
10
1
Rock/MORB
NM-7
NM-6
NM-5
NM-2
Continental Arc Andesites
Ba
Rb
K
Nb
La
Ce
Sr
P
Sm
Zr
Ti
Y

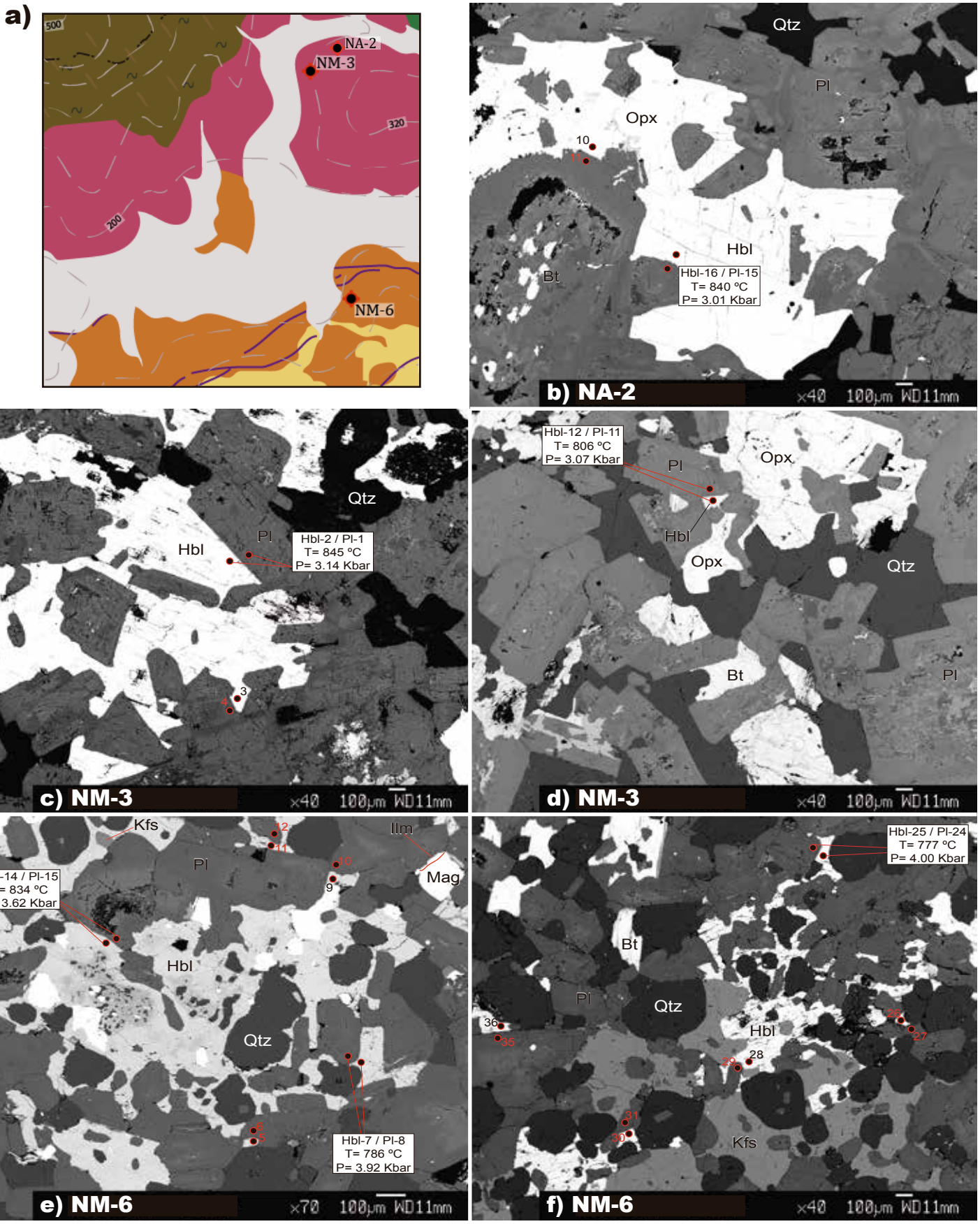
a)
500
320
200
NA-2
NM-3
NM-6
Qtz
Pl
Opx
10
11
Hbl
Bt
Hbl-16 / Pl-15
T= 840 °C
P= 3.01 Kbar
b) NA-2
×40 100µm WD11mm
Qtz
Hbl
Pl
Hbl-2 / Pl-1
T= 845 °C
P= 3.14 Kbar
3
4
c) NM-3
×40 100µm WD11mm
Hbl-12 / Pl-11
T= 806 °C
P= 3.07 Kbar
Pl
Opx
Hbl
Opx
Qtz
Bt
Pl
d) NM-3
×40 100µm WD11mm
Kfs
12
11
Ilm
Pl
10
9
Mag
Hbl-14 / Pl-15
T= 834 °C
P= 3.62 Kbar
Hbl
Qtz
6
5
Hbl-7 / Pl-8
T= 786 °C
P= 3.92 Kbar
e) NM-6
×70 100µm WD11mm
Hbl-25 / Pl-24
T= 777 °C
P= 4.00 Kbar
Bt
Pl
Qtz
36
35
Hbl
26
27
29
28
31
30
Kfs
f) NM-6
×40 100µm WD11mm

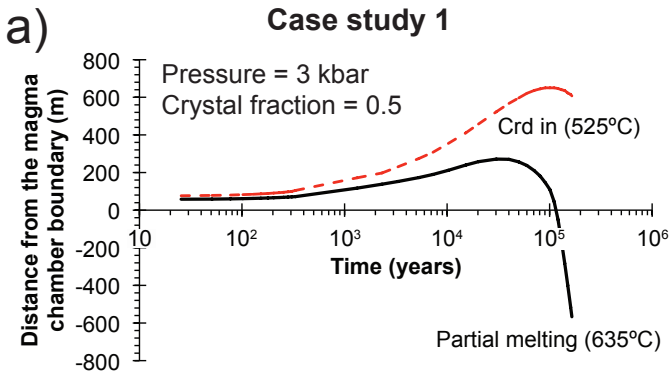
a)
Case study 1
Pressure = 3 kbar
Crystal fraction = 0.5
Crd in (525ºC)
Partial melting (635ºC)
Distance from the magma chamber boundary (m)
Time (years)

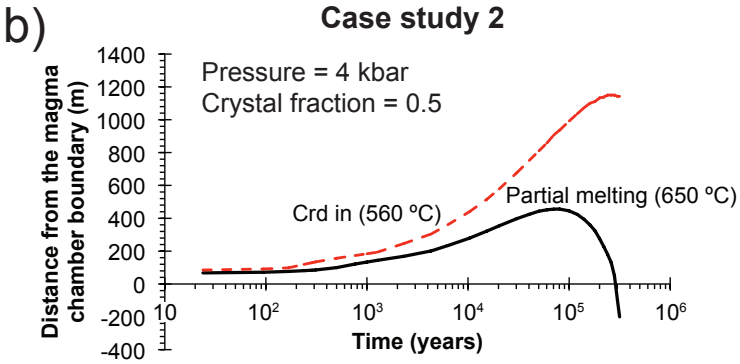
b)
Case study 2
Pressure = 4 kbar
Crystal fraction = 0.5
Crd in (560 ºC)
Partial melting (650 ºC)
Distance from the magma chamber boundary (m)
Time (years)

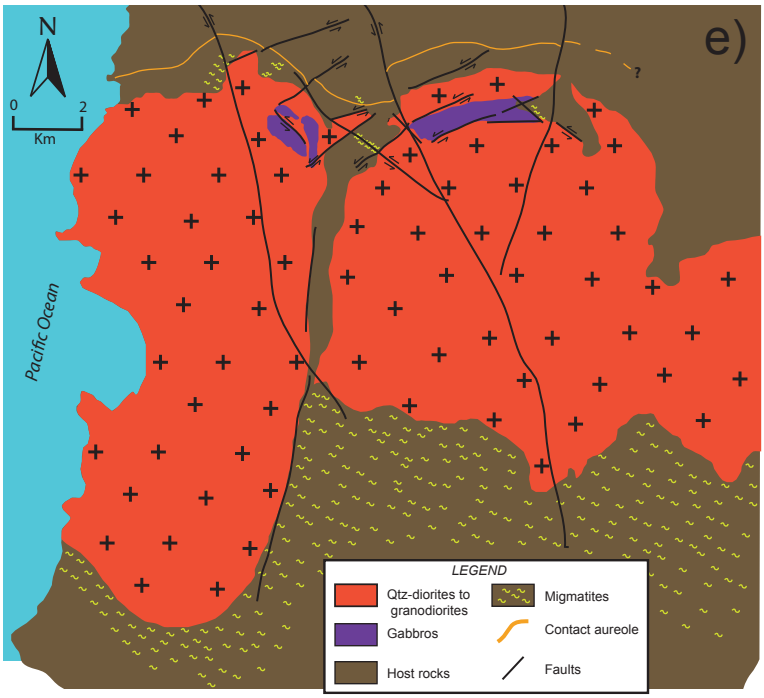
e)
N
0
2
Km
Pacific Ocean
LEGEND
Qtz-diorites to granodiorites
Gabbros
Host rocks
Migmatites
Contact aureole
Faults

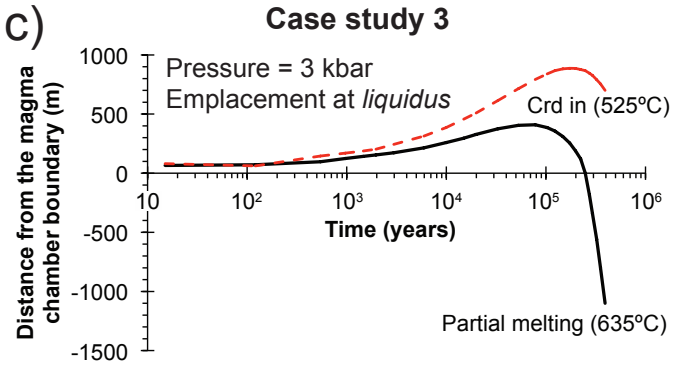
c)
Case study 3
Pressure = 3 kbar
Emplacement at liquidus
Crd in (525ºC)
Partial melting (635ºC)
Distance from the magma chamber boundary (m)
Time (years)

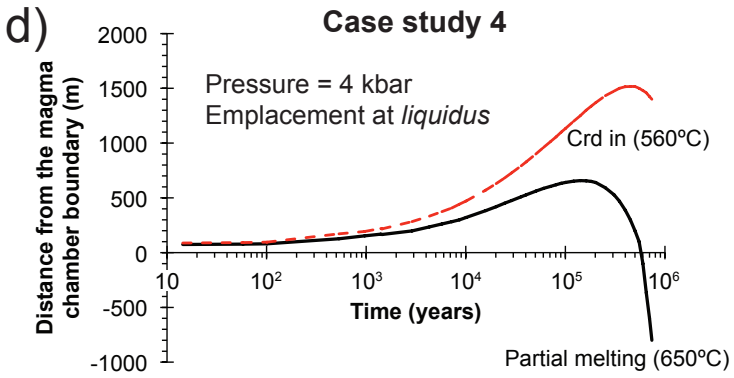
d)
Case study 4
Pressure = 4 kbar
Emplacement at liquidus
Crd in (560ºC)
Partial melting (650ºC)
Distance from the magma chamber boundary (m)
Time (years)

Table 1

Whole-rock analyses of major and trace elements of granitoids of the northern area of the Flamenco pluton

Rock type	Tonalite	Crd-Grd*	Qtz-Diorite	Gabbro	Granodiorite			Tonalite
Sample	NM-1	NM-2	NM-3	NM-4	NM-5	NM-6	NM-7	NM-8
(Wt%)								
SiO_2	59,59	65,75	55,72	47,98	67,26	65,17	64,83	63,82
TiO_2	0,73	0,56	0,75	0,91	0,4	0,67	0,74	0,59
Al_2O_3	15,78	16,05	17,76	19,82	15,58	15,16	15,69	15,7
Fe_2O_3	2,01	1,86	4,04	3,83	2,23	2,95	3,41	2,21
FeO	6,52	3,86	7,48	9,37	3,87	4,95	3,84	5,28
MgO	3,46	2,42	4,32	6,2	1,27	2,06	1,78	2,63
MnO	0,14	0,06	0,16	0,2	0,08	0,11	0,08	0,13
CaO	6,43	4,43	8,26	10,37	4,03	4,62	4,98	5,74
Na_2O	2,74	3,92	2,69	2,16	3,47	3,39	2,96	3,27
K_2O	1,44	1,54	0,71	0,18	2,59	2,35	3,36	1,48
P_2O_5	0,12	0,17	0,1	0,12	0,15	0,13	0,21	0,16
LOI	2,23	0,73	1,11	1,55	0,75	0,75	0,99	0,53
Total	99,18	99,49	99,06	98,86	99,45	99,36	99,46	99,33
(ppm)								
Rb	58	48	30	5	107	88	153	51
Sr	188	379	192	237	174	160	251	274
Y	28	17	23	19	29	32	29	21
Zr	119	136	60	-	198	173	260	138
Nb	6	8	5	6	10	6	9	7
Ba	168	-	2	46	275	-	-	172
La	1,37	2,77	1,48	1,04	0,28	1,64	3,07	0,56
Ce	7,2	11	2,84	2,22	8,57	1,94	14,3	10,5
Sm	1,48	0,83	1	0,68	0,98	0,12	1,23	1,29
Lu	0,35	0,22	0,43	0,32	0,3	0,12	0,17	0,57

*Grd: Granodiorite

Table 2

Plagioclase–Hornblende thermobarometry results

			2 Kbar	4 Kbar	Schmidt		A&S
Sample	Hbl	Pl	T (ºC)	T (ºC)	T (ºC)	P (Kbar)	T (ºC)
NA-2	NA2-16	NA2-15	837	844	840	3,01	830
	NA2-10	NA2-11	831	840	835	2,84	824
	NA2-2	NA2-7	821	828	824	2,86	816
	NA2-4	NA2-3	835	843	839	3,00	829
NM-3	NM3-2	NM3-1	842	848	845	3,14	836
	NM3-3	NM3-4	814	823	820	3,32	810
	NM3-12	NM3-11	802	809	806	3,07	799
NM-6	NM6-5	NM6-6	795	801	801	4,18	796
	NM6-7	NM6-8	780	787	786	3,92	781
	NM6-9	NM6-10	795	799	798	3,61	794
	NM6-11	NM6-12	790	796	796	3,80	790
	NM6-14	NM6-15	829	835	834	3,62	826
	NM6-25	NM6-24	770	777	777	4,00	772
	NM6-26	NM6-27	785	792	794	4,57	787
	NM6-28	NM6-29	792	798	799	4,06	792
	NM6-30	NM6-31	771	778	778	4,18	773
	NM6-36	NM6-35	794	798	796	3,18	792
	NM6-5*	NM6-3*	897	904	904	4,18	889

T (°C): HB2 temperature in Holland and Blundy (1994).
2 and 4 Kbar: results based on an arbitrary pressure.
Schmidt: pressure-based results according to Schmidt's (1992).
A&S: pressure-based results according to Anderson and Smith's (1995).
*This Hbl-Pl pair is not in contact. Pl core and unzoned Hbl thermobarometry

Table 3. Case studies designed for the thermal modelling

Case study	1	2	3	4
Temperature of emplacement (ºC)*	992	1007	1141.6	1159
Depth of emplacement (km)	11	14.4	11	14.4
Thermal conductivity (W/mºC)	1.5	1.5	1.3	1.3
Specific heat capacity (J/kgK)*	1259	1271	1249	1249
Crystal fraction	0.5	0.5	0	0
Volume (km^3)	62.83	62.83	62.83	62.83
Density (kg/m^3)*	2641	2655	2524	2541

*Parameters estimated by Rhyolite-MELTS